Electronic excited states of planar vs bowl-shaped polycyclic aromatic hydrocarbons in interaction with water clusters: a TD-DFT study

Nadia Ben Amor, Salimata Konate, Aude Simon

Noname manuscript No.
(will be inserted by the editor)

Electronic excited states of planar vs bowl-shaped polycyclic aromatic hydrocarbons in interaction with water clusters: a TD-DFT study

Nadia Ben Amor · Salimata Konate · Aude Simon

Received: date / Accepted: date

Abstract In an astrochemical and environmental context, this work constitutes a step forward in understanding the photo-reactivity of polycyclic aromatic hydrocarbons (PAHs) with water molecules and in water ice under irradiation with low energy photons. The role of charge transfer states PAH^+-H_2O^- has been proposed, motivating the study of the electronic excited states up to about 6 eV of planar and bowl-shaped PAHs, namely pyrene $C_{16}H_{10}$ and corannulene $C_{20}H_{10}$, interacting with water clusters of different sizes and orientations, using a time-dependent density functional theory approach. In the case of pyrene, the systematic occurrence of low energy excitations from π orbitals to diffuse orbitals located on some water molecules, mixed with the Rydberg orbitals (R/wat), was found. Such excitations are more numerous and possess larger oscillator strengths when (i) the number of water molecules increases up to representing a first layer of hexagonal water ice and (ii) for the arrangements leading to the lower vertical ionisation potential values. In this case, the /wat orbitals are located on the most external H atoms and they may

Nadia Ben Amor
Laboratoire de Chimie et Physique Quantiques (LCPQ), Fédération FERMI, Université de Toulouse UT3 & CNRS, UMR5626, 118 Route Narbonne, F-31062 Toulouse, France
E-mail: benamor@irsamc.ups-tlse.fr

Salimata Konate
Laboratoire de Chimie et Physique Quantiques (LCPQ), Fédération FERMI, Université de Toulouse UT3 & CNRS, UMR5626, 118 Route Narbonne, F-31062 Toulouse, France

Aude Simon
Laboratoire de Chimie et Physique Quantiques (LCPQ), Fédération FERMI, Université de Toulouse UT3 & CNRS, UMR5626, 118 Route Narbonne, F-31062 Toulouse, France
E-mail: aude.simon@irsamc.ups-tlse.fr

also mix with $\pi^\star$ orbitals. This accounts for the efficient reactivity of pyrene with water in water ice. In the case of corannulene, the main result is that, for the $C_{20}H_{10}(H_2O)_3$ isomer formed in a noble gas matrix, where $(H_2O)_3$ interacts with the concave face of corannulene, no $\pi \rightarrow$R/wat transition is observed. It is in line with the lack of reactivity of corannulene with water in a noble gas matrix.

Keywords Electronic excited states · Charge transfer · Rydberg states · TD-DFT · water clusters · polycyclic aromatic hydrocarbons

1 Introduction

The study of interactions between polycyclic aromatic hydrocarbon (PAH) molecules and water aggregates is of tremendous interest in atmospheric science, astrophysics and astrochemistry. Indeed, PAH molecules can be found in our Earth atmosphere where they can become part of atmospheric aerosols, which are known to have a significant impact on the Earth's radiation [1]. PAH clusters can indeed be regarded as good models for such aerosols on which small atmospheric molecules such as water condense and grow [2]. Such aerosols play an important role in atmospheric chemistry, as they act as surface catalysts for heterogeneous reactions [3,4].

Interstellar PAHs have been of significant interest since the proposal in the eighties that they were the carriers of the Aromatic Infrared Bands (AIBs), a set of mid-IR emission bands observed in many regions of the interstellar medium (ISM) [5,6]. They would account for up to 20 % of the total carbon [7,8]. Although PAHs have been believed to be ubiquitous in the ISM for decades, motivating experimental and theoretical spectroscopic studies in order to identify a specific PAH molecule [8], it is only very recently that specific PAH molecules, the two isomers of cyano-naphthalene, have been successfully detected based on their rotational spectra [9]. In the denser regions of the ISM, PAHs may freeze on the icy mantle of interstellar dust grains [10] where they can interact with other molecules like water and undergo physical and chemical processes induced by UV photons emitted by nearby stars such as oxidation reactions [11].

Clusters in space or atmospheric conditions are difficult to study experimentally due to low binding energy leading to the need to trap the species in low temperature conditions. Water-PAH neutral clusters were studied in cryogenic environments such as noble gas matrices [12–16]. They were also formed in the gas phase and characterised by rotational spectroscopy experiments complemented with *ab initio* calculations [17–19].

This work enters the general context of the need to understand the mechanisms underlying the photo-reactivity of PAHs with water molecules in a cold environment which can be a noble gas matrix or water ice. Photo-reactivity of planar PAHs, namely pyrene $C_{16}H_{10}$ and coronene $C_{24}H_{12}$, with water molecules

in a noble gas matrix and on ice, was experimentally observed under irradiation with low energy photons ($\lambda > 235\,\mathrm{nm}$). This led to the production of oxygen-containing PAH products such as ketones and possibly quinones [12, 13]. On the opposite, no photo-reactivty was observed in the case of the bowl-shaped PAH corannulene $C_{20}H_{10}$: only $(C_{20}H_{10})(H_2O)_n$ (n=2,3) complexes were formed and did not undergo any photo-reaction [16].

The experimental results on the photo-reactivity of PAH with water in noble gas matrix led us to investigate the structures of $PAH(H_2O)_n$ inside an argon matrix, describing explicitely all the degrees of freedom at the mixed density functional based tight-binding/force field (DFTB/FF) levels of theory [15, 16]. Our results show that in the case of planar PAHs, the geometries with the water molecules interacting via their oxygen atoms with the H of the PAH in the plane of the PAH ("side isomers" with one or two water molecules) are the most stable ones and are expected to be formed in the matrix [15]. On the opposite, in the case of corannulene the most favorable situation is when the water clusters (trimer and possibly dimer) interact via their H atoms with the π cloud close to the symmetry axis of corannulene, namely "face" isomers [16].

One hypothesis to account for the photo-reactivity of planar PAHs with water is that it could be ion-mediated, even at low energy [20]. Experimental investigations combined with computational studies have shown that the ionisation of PAHs adsorbed on water ice requires about 1.5 to 2.0 eV less energy than in the case of isolated PAHs [21, 22], and that the resulting PAH radical cations would be particularly stable over time [23]. That could be accounted for by the fate of the electrons released by the ionisation, that would not be free electrons but would attach to H_2O molecules or free radicals such as OH formed during ice photolysis [23].

The physical and chemical processes underlying the lowering of the PAH ionisation energies in water ice motivated theoretical studies. We showed using DFTB calculations with charge constraint that the vertical ionisation potential (VIP) of the PAH was modified by less than 0.8 eV upon adsorption on different types of ices, and that the VIP variations depended on the local organisation on the water molecules at the ice surface interacting with the PAH [24]. The interaction of the PAH with O-H dangling bonds (-H at the surface of water ice) favors an increase of the VIP while the interaction of the PAH with O atoms of the ice surface favors a decrease of the VIP. However, the amplitude of the VIP variations is not sufficient to account for the experimental results. In order to do so, one must assume that the electrons will recombine with water molecules or OH radicals. Theoretical studies, *i.e.* density functional theory (DFT) study of water clusters and extrapolation law to infinite size, have estimated the electron affinity of water ice to be in the 1.65-3.3 eV range ([25] and references therein) and that of OH trapped in ice to be 5.06 eV (using the isodensity polarised continuum model) [22].

The role of a long lived excited electronic charge transfer (CT) state PAH^+-H_2O^- lower in energy than the PAH VIP by more than 2 eV could account for the experimental results. If this hypothesis is correct, such a state is expected to exist for planar PAHs but not for the bowl-shape corannulene, that does not undergo any photo-reaction with water. This motivated the present investigation dedicated to the study of the electronic excited states of $PAH(H_2O)_n$ systems, focusing on one planar and one non planar PAHs, namely pyrene $C_{16}H_{10}$ and corannulene $C_{20}H_{10}$ respectively. In the case of corannulene, we studied the electronic states for up to three water molecules, such stoichiometry being expected in a noble gas matrix [16]. In the case of pyrene, the interaction with one water molecule in a matrix is expected, as it is a planar PAH similar to coronene [15] and this stoichiometry is studied in the present work as a model case system. Interestingly, the photo-reactivity of pyrene in water ice is more efficient than in a noble gas matrix [13]. As a result, in the case of pyrene only, we increased the size of the water cluster so as to mimic its interaction with water ice. Due to the size of the systems, time dependent (TD)-DFT methods were considered.

We benchmarked the approach focusing on the smallest aromatic carbon molecule (benzene) [26]. In the latter work, the electronic spectra of a benzene C_6H_6 molecule in interaction with water clusters of different structural organisations and different sizes, from one to fifty water molecules, were computed, and a detailed analysis of the transitions up to $\sim$ 8 eV was performed. The geometries were extracted from two benzene-hexagonal (Ih) ice configurations leading to maximum (Geo_{IEI} series) and minimum (Geo_{IED} series) ionisation energies of the benzene-water clusters. For all systems, the electronic spectra were computed at the TD-DFT level in conjunction with an appropriate basis set containing diffuse and polarisation orbitals on the atoms and describing the Rydberg states of benzene. The approach was carefully benchmarked against multi-state complete active space perturbation theory at the second order (MS-CASPT2) [27] results for the smallest systems, up to six water molecules. For the smallest systems, our results clearly showed the influence of the clusters' structures on the spectra. For the Geo_{IED} series, we found low energy $\pi \rightarrow$Ry/wat transitions of non negligible intensity describing the promotion of one electron to a Rydberg orbital having an important contribution on the water molecule whose oxygen points towards the H atom of C_6H_6. For larger systems, $\pi \rightarrow$Ry/wat transitions below 7 eV were observed for all configurations but more numerous for those from the Geo_{IED} series. The difference with the small systems is that the Rydberg orbitals become mainly developed on the H atoms of the water molecules at the edge of the cluster. Such $\pi \rightarrow$Ry/wat transitions, that can be regarded as CT states, were found more than 2 eV below the IP of C_6H_6. As a result, such states could be formed upon irradiation of the systems with low energy photons as achieved in the photo-reactivity experiments [12,13]. In the present article, we aim to investigate whether such states are present in the case of pyrene, which is photo-reactive [12], and not in the case of corannulene, which remains unreactive upon irradiation [16].

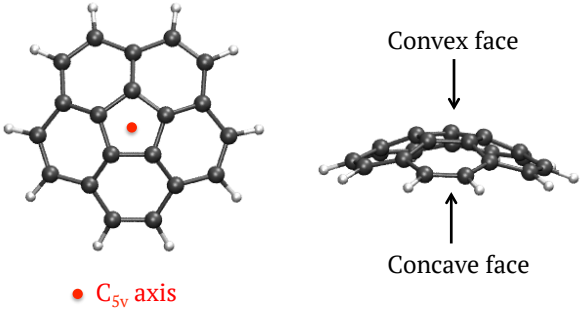

Fig. 1 Geometry of bare corannulene

The computational approaches are described in Section 2. The results are reported and discussed in Section 3.

2 Computational methods

2.1 Geometries

Corannulene
The corannulene geometry is optimised in an argon matrix at the DFTB/FF level of theory [16] consistently with the other systems studied in this work. The DFTB/FF hybrid scheme was developed in order to provide a good description of water-hydrocarbon clusters inside a noble gas matrix with an explicit description of all the atoms. The water -hydrocarbon clusters are described using an improved self-consistent-charge (SCC)-DFTB hamiltonian using charge model 3 (CM3) charges instead of Mulliken charges in the orginal SCC-DFTB hamiltonian, and including a dispersion empirical term. The interactions between the atoms of a noble gas matrix are described at the FF level. Further details regarding the development and benchmark of the hybrid DFTB/FF scheme can be found in references [28,29] and applications to PAH-water clusters in references [15,16].

As can be seen in Fig. 1, corannulene $C_{20}H_{10}$ presents a concave and convex face. Water molecules can then interact with the concave or convex face or with the H atoms on the side of corannulene. These positions are respectively named "cav", "vex" and "side" in the rest of the manuscript. For two or three water molecules, combined situations may occur, with one water on the side and one or two water molecules on the concave or convex face. These situations are designated "cav-side" or "vex-side" in the rest of the manuscript. All possibilities of interactions between one to three water molecules with corannulene in a noble gas matrix were previously investigated at the DFTB/FF

level of theory and local optimisations were performed [16]. The most stable conformers obtained for each situation are reported in Fig. 2 along with their relative energies for a given stoichiometry. From the comparison between experimental and theoretical results, we showed that the 3-cav geometry was formed in a noble gas matrix [16] while the 2-vex and 2-cav ones could not be excluded. The noble gas atoms were removed for the TD-DFT studies.

Pyrene

The geometry used for the benchmark on bare pyrene was optimized at the DFT level of theory (B3LYP/6-31+G*) and taken from a previous study on the valence excited states for this molecule which were performed using this geometry [30].

In order to get insight into the influence of the orientation of one water molecule on the electronic spectrum of pyrene, we investigated the electronic excited states of two model isomers for $C_{16}H_{10}(H_2O)_1$): one for which the water molecule interacts with the face isomer of pyrene (namely GEO1_IP$_{Max}$) and one for which it interacts on the side of the pyrene molecule (namely GEO1_IP$_{Min}$). The geometries were locally optimized at the DFTB level of theory using CM3 charges and dispersion correction, as in the case of corannulene. In the case of pyrene, no optimisation in a matrix using the DFTB/FF hamiltonian was performed. However, from our previous study of coronene-water clusters inside a noble gas matrix, coronene being a planar PAH similar to pyrene, the GEO1_IP$_{Min}$ "side" geometry is the one expected to be formed in a noble gas matrix [15].

As mentioned in the introduction, the photo-reactivity of pyrene occurs in a rare gas matrix, but is reinforced when pyrene is embedded in water ice. Therefore in the case of pyrene, we aim at investigating the influence of the number of water molecules and their arrangements up to reaching a cluster size mimicking the water ice. The geometries of pyrene interacting with two or three molecules were then retrieved from two structures of pyrene adsorbed on crystalline hexagonal (Ih) water ice, treated as a finite size large cluster (see Fig. 3) optimized at the DFTB level of theory [24]: one structure, namely GEO_IP$_{Max}$ in Fig. 3, for which the VIP is maximum (8.07 eV [24]) and second one, namely GEO_IP$_{Min}$ in Fig. 3, for which the VIP is minimum (6.15 eV [24]). Regarding the DFTB hamiltonian employed for such clusters, the default (Mulliken) charges originally employed in the SCC-DFTB scheme were improved and replaced by "Weighted Mulliken Charges" and an empirical dispersion term was added. This led to a significant improvement of the description of intermolecular water-water interactions both for small water clusters and large ones mimicking water ice, and PAH-water interactions. This was validated against the results of MP2 calculations as described in reference [24]. From the original large optimized clusters, only the closest water molecules to pyrene were retained, leading to two series of structures reported in Fig. 4, GEOn_IP$_{Max}$ and GEOn_IP$_{Min}$ where n is the number of water molecules (n=2,3, 15 or 16). In the case of the GEOn_IP$_{Min}$ series, for n=2 (n=3 respectively), we imposed that one water molecule (two respectively)

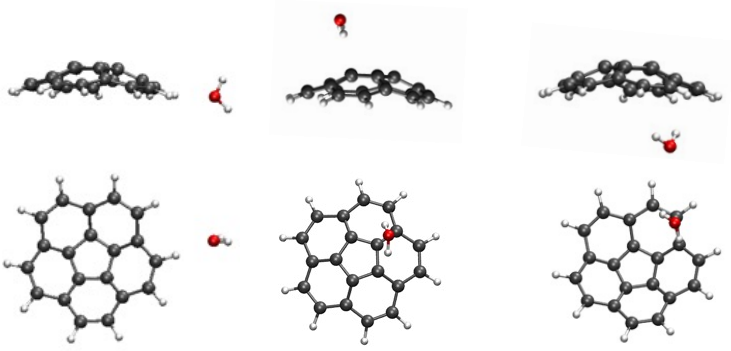

(a) 1-side (0.0) (b) 1-vex (+0.5) (c) 1-cav (+1.8)

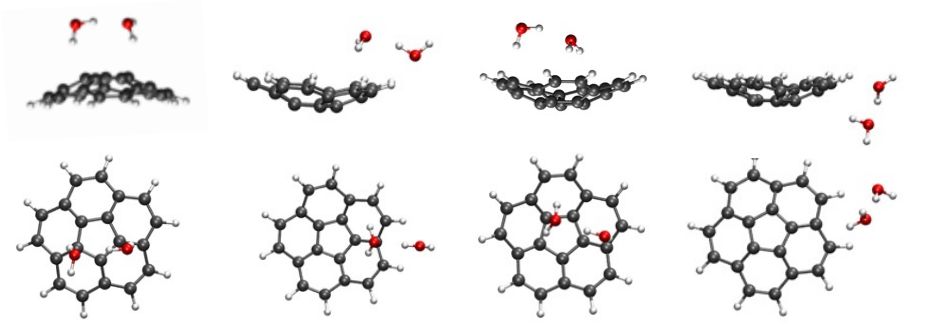

(a) 2-vex (0.0) (b) 2-cav-side (+2.3) (c) 2-cav (+2.5) (d) 2-vex-side (+12.9)

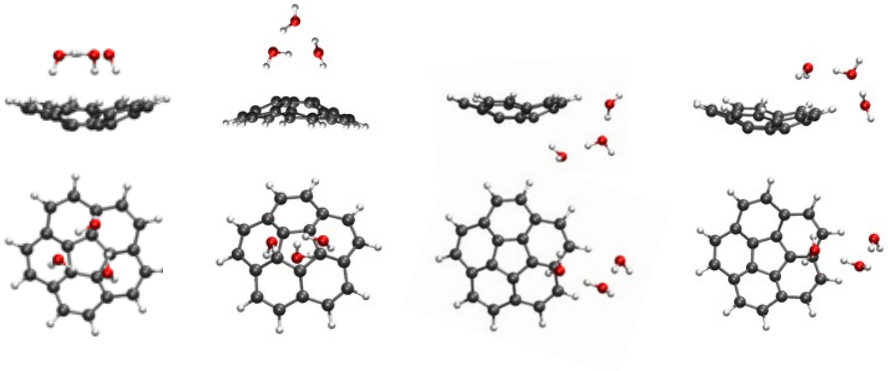

(a) 3-cav (0.0) (b) 3-vex (+4.1) (c) 3-vex-side (+7.1) (d) 3-cav-side (+9.3)

Fig. 2 Adapted from ref. [16] Geometries of $(C_{20}H_{10})(H_2O)_{1\text{-}3}$ isomers and energetic order in the noble gas matrix (relative energies are expressed in kJ/mol in parenthesis.)

interacted via their oxygen atoms with the hydrogen atoms of pyrene in order to analyse the differences of the electronic transitions with those of the corresponding GEOn_IP$_{Max}$ (n=2,3) isomers. The distances between $(H_2O)_{n=2,3}$ and pyrene are given in the SI.

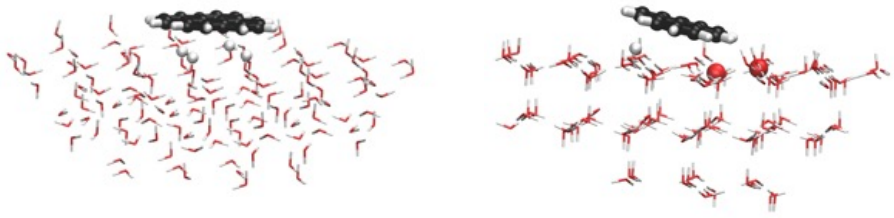

(a) GEO_IP$_{Max}$ (8.07 eV) (b) GEO_IP$_{Min}$ (6.15 eV)

Fig. 3 Adapted from ref. [24]. Geometries of $C_{16}H_{10}$ adsorbed on Ih water ice. Left: IP max and right: IP min) In parenthesis, the vertical IP values obtained at the DFTB/CI level from ref [24] are reported. At this level of theory, that of pyrene was found to be 7.41 eV.

2.2 Methods and basis sets

The basis set used for the TD-DFT studies is, as in our previous study[26], the Split Valence Polarization (SVP) bases of Dunning-Hay [31], to which a diffuse function was added for each atom. In presence of Rydberg states, specific diffuse Gaussian basis sets are used and placed at the center of charge of the cation [32]. These functions are limited to 2s2p2d1f and correspond to the diffuse functions defined by Dunning for the carbon atom, with an additional f function (exponent 0.012). In the following, the Rydberg basis set is named Ry, the combination with the PAH basis set DunRy. Additional calculations are performed enlarging the basis set of the pyrene atoms to 6-311++G(2p,2d) [33,34]. Since for the pyrene molecule the TD-DFT results are compared to MS-CASPT2 ones, the same Atomic Natural Orbitals (ANO) [35] basis sets are also used for the TD-DFT calculations. However, since the effect of the basis sets is small ($\leq$ 0.06 eV), these results are only given in the SI, as are the basis sets used.

Due to the size of the studied systems, TD-DFT is the most suitable method since it has, moreover, given satisfactory results in our previous study on benzene-water clusters [26]. Some tests were performed in order to validate the functionals on the pyrene and corannulene bare molecules. The presence of Rydberg states and CT states between PAH and water molecules placed the B3LYP[36–39] functional in difficulties and more suitable ones were tested: CAM-B3LYP [40], M06-2X [41] and wB97X [42]. In order to reach the CT state(s), 20 excited states were computed. The oscillator strengths are reported only if they are larger than 10^{-3}.

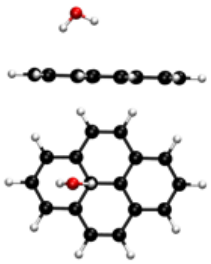

(a) GEO1_IP$_{Max}$ (7.48 eV)

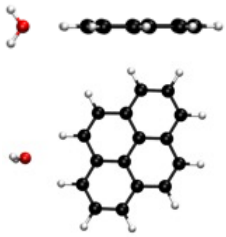

(b) GEO1_IP$_{Min}$ (6.97 eV)

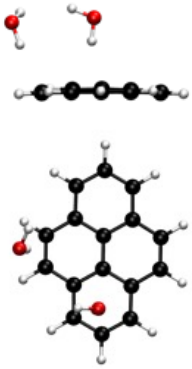

(c) GEO2_IP$_{Max}$ (7.60 eV)

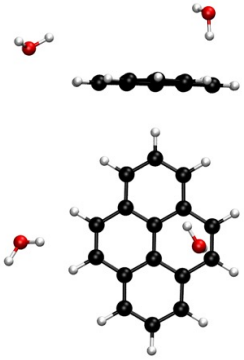

(d) GEO2_IP$_{Min}$ (7.47 eV)

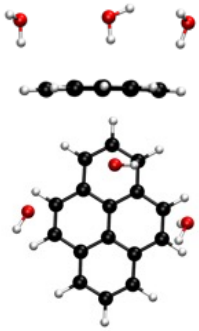

(e) GEO3_IP$_{Max}$ (7.71 eV)

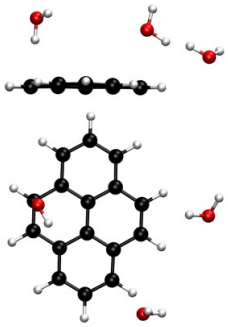

(f) GEO3_IP$_{Min}$ (7.34 eV)

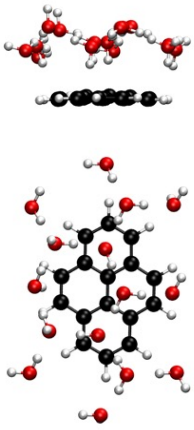

(g) GEO15_IP$_{Max}$ (7.97 eV)

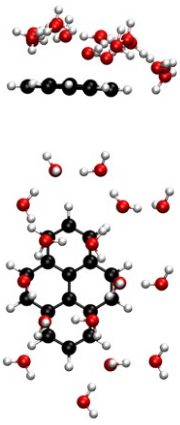

(h) GEO16_IP$_{Min}$ (6.54 eV)

Fig. 4 Geometries of $(C_{16}H_{10})(H_2O)_n$ isomers, n=1-3,15 or 16 from top to bottom, for which the electronic excited states were computed. The geometries on the left-hand side correspond to GEOn_IP$_{Max}$ structures and those to the right to GEOn_IP$_{Min}$ structures (see main text in section 2 for explanations.) The VIPs computed in this work are reported in parenthesis.

Complete Active Space Self Consistent Field (CASSCF) [43] and MS-CASPT2 [27] methods were used in a previous work [30] for the determination of the excitation energies of the pyrene valence states. These calculations were performed in the D_{2h} symmetry group and based on the ANO basis sets [35]. In the present study, as the goal is to study also the Rydberg states, it was necessary to add diffuse functions as it was the case for the TD-DFT calculations. The details of the procedure are developed in the SI. The TD-DFT results concerning the valence states are compared to the already published MS-CASPT2 calculations [30]. However, comparison of the TD-DFT results using the different basis sets can be found in the SI.

Concerning the Rydberg states, the first three, a^1B_{1g} (s), a^1B_{3u} (py), and a^1A_u (pz) were determined by using Restricted Active Space SCF (RASSCF [44,45]) and PT2 (RASPT2 [46,47]) methods. In the RASSCF, the active space is separated in three subspaces: i) RAS1 with doubly occupied orbitals in which a limited number of holes is allowed, ii) RAS2 corresponds to the standard complete active space, iii) RAS3 is the subspace containing virtual orbitals where a given number of particles could be created. In the present case, no orbital is placed in subspace RAS1 while the orbitals included in the RAS2 subspace are the 16 π orbitals, at the limit of the possibilities of this type of calculations. However, thanks to the symmetry of the pyrene molecule, it has been possible to add one Rydberg orbital (s, py or pz) in the RAS3 subspace where one electron can be created. This procedure allows the description of a Rydberg excited state as a π excitation to a Rydberg orbital. As a consequence, three different sets of active spaces are defined following the Rydberg orbital included, and the excitation energies are given by calculating the difference of the ground and excited states energies obtained with the same set of active spaces.
These reference data will allow to benchmark TD-DFT calculations.
The energies of the cations at the geometries of the corresponding neutral clusters were also computed using the CAM-B3LYP functional and the DunRy basis set. The VIPs as reported in this article consist in the energy difference between this energy and that of the optimized neutral cluster at the same level of theory.

The RASSCF/RASPT2 calculations were carried out with the 7.8 MOLCAS package [48–50]. The TD-DFT calculations and the Natural Transitions Orbitals (NTOs) [51] were performed using the Gaussian16 suite of programs [52] and drawn with the associated software Gaussview6.

3 Results and discussion

3.1 Benchmarks

The spectra of the electronic excited states of bare pyrene $C_{16}H_{10}$ (Figure 5) obtained with the different functionals B3LYP, M06-2X, CAM-B3LYP and wB97X are compared to MS-CASPT2 results for $\pi \rightarrow \pi^\star$ states [30] and to

RASPT2 ones for Rydberg states (see Table 1). The $\pi \rightarrow \pi^\star$ MS-CASPT2 excitation energies are in good agreement with the experimental data (maximum deviation ≈ 0.2 eV).

Due to the size of the active space, the number of determinants is very large, more than 20 millions, therefore only the coefficients of determinants greater than 0.05 are considered for the evaluation of mono- or di-excited character of the wave function. Four excited states have a weight on the mono-excited determinants lower than 0.6: a^1A_g (0.43), b^1A_g (0.53), c^1B_{3g} (0.48) and c^1A_g (0.58). If we compare the TD-DFT excitation energies to the MS-CASPT2 values, the first point to be mentioned is that B3LYP functional gives the closest excitation energies for the valence $\pi \rightarrow \pi^\star$ states, with a maximal deviation of 0.5 eV for the c^1B_{3g} state. Five states deviate by 0.2 eV or more: the four states with a pronounced di-excited character and the a^1B_{2u} excited state. The latter is the first excited state at the B3LYP level but this corresponds to an inversion of the two first excited states that does not occur with the other functionals. However, all the other functionals present a larger deviation with a maximum difference of 1 eV for CAM-B3LYP and M06-2X (a^1A_g) and 1.35 eV for wB97X (c^1A_g). Considering now the Rydberg states, B3LYP is not the most accurate functional as the comparison with the RASPT2 values shows an underestimation of 0.35-0.5 eV. The wB97X functional overestimates the values ($\approx$0.6 eV). Finally, the smallest difference is shown for the other functionals, *i. e.* less than 0.1 eV for CAM-B3LYP and less than 0.2 eV for M06-2X. Globally, the mean absolute error (MAE) over all states amounts to 0.46 eV for CAM-B3LYP, 0.5 eV for M06-2X, 0.28 eV for B3LYP and 0.78 eV for wB97X.

These functionals were also used for bare corannulene $C_{20}H_{10}$ (Table 2) and the same trends were observed for the excitation energies of the $\pi \rightarrow \pi^\star$ states compared to experimental values. Unfortunately, the number of π orbitals is now too large to allow the use of CASSCF/CASPT2 methods. In conclusion, even though the MAE is lower for B3LYP funtional, the necessity to describe as accurately as possible the charge transfer processes and the Rydberg states led us to adopt the CAM-B3LYP functional for the study of the electronic states of PAHs in interaction with water clusters.

The benchmarks on the basis sets are presented in the SI as the effect is small ($\leq$ 0.06 eV).

3.2 Results for corannulene

Regarding corannulene, the inherent difference with pyrene is that, due to its bowl shape, it possesses low energy super atom molecular orbitals (SAMOs). [61–66] These were first characterized for buckminsterfullerene C_{60} [61].
The nature and the energies of the transitions up to $\sim$6 eV for $(C_{20}H_{10})(H_2O)_n$ are reported in Tables 3,4 and 5 for n=1,2 3 respectively and compared to the results for bare $C_{20}H_{10}$. The VIPs are also reported as well as the number

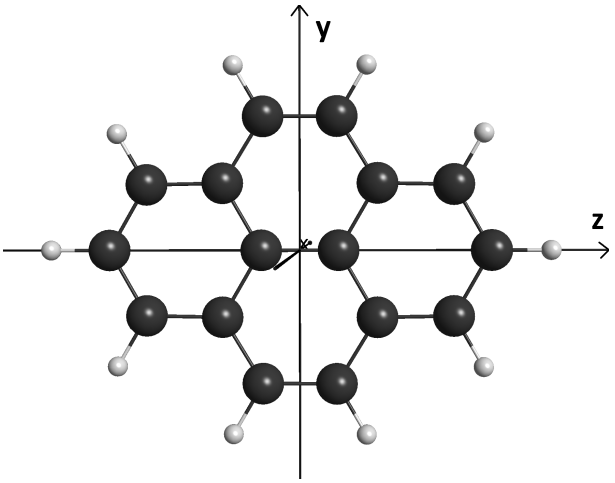

Fig. 5 Geometry of bare pyrene

of distances shorter than 3Å between the H (resp. O) atoms of the water molecules and the C (resp. H) atoms of corannulene, designated Nb(H–C) (resp. Nb(O–H)) in Tables 3,4 and 5.

As can be seen in these tables, the first eight states of bare and corannulene-water systems correspond to $\pi \rightarrow \pi^\star$ excitations and present very similar excitation energies. The following two states also correspond to $\pi \rightarrow \pi^\star$ excitation with a small contribution of a $\pi \rightarrow$ D (Diffuse) excitation, at the exception of the bare corannulene, and of the 1,3-vex and 3-cav-side configurations, where the transitions remain pure $\pi \rightarrow \pi^\star$ excitations.

A precise characterization of the diffuse orbitals (designated D in the Tables) was difficult. The SAMO vs Rydberg distinction, based on their spatial extension and shape was difficult to disentangle. These orbitals have no contribution on the water molecules except in very few cases (see NTOs on Fig. 6) where this contribution is minor, except for the 1-side conformer. In the 1-side case, the transition at 5.64 eV involves a diffuse orbital on the water molecule, designated /wat in the rest of the manuscript. In the 2-cav-side, 2-vex-side, 3-cav-side and 3-vex-side configurations, the diffuse orbitals appear to have small coefficients on the diffuse orbitals of the H atoms of the water molecules interacting via their H atoms with the π cloud of corannulene. The $\pi \rightarrow$D$/\pi^\star$ transitions involve several excitations and the weight of the main NTO does not exceed 75 %. Interestingly, for the stable 3-cav stable configuration very likely to be formed in noble gas matrices [16], the diffuse orbitals do not involve the water molecules. It is also the case of the 2-cav, while regarding the 2-vex, only a very minor contribution was found for transitions 15 to 17. The presence of the 2-cav and 2-vex aggregates in a noble gas matrix can indeed not be excluded [16].

Table 1 Bare pyrene: effect of the DFT functional. Experimental data, and TD-DFT, MS-CASPT2/RASPT2 excitation energies (eV) and oscillator strengths from the ground state

Valence $\pi \rightarrow \pi^\star$ states

State	CAM-B3LYP DunRy	M06-2X DunRy	B3LYP DunRy	wB97X DunRy	MS-CASPT2 ANO-RCC[b]	Exp [a]
a^1B_{2u}	3.92	3.95 (10^{-3})	3.71	4.01	3.43 (10^{-3})	3.34-3.42
a^1B_{1u}	3.94 (0.340)	4.00 (0.355)	3.64 (0.271)	4.10 (0.369)	3.82 (0.38)	3.65-3.85
a^1B_{3g}	4.68	4.71	4.26	4.90	4.15	4.12-4.23
b^1B_{2u}	5.00 (0.427)	5.00 (0.417)	4.55 (0.271)	5.27 (0.538)	4.44 (0.48)	4.55-4.69
a^1A_g	5.45	5.45	4.89	5.75	4.47	4.54-4.61
b^1B_{3g}	5.03	5.09	4.57	5.28	4.53	4.29
b^1A_g	5.62	5.65	5.12	5.85	4.94	5.16
c^1B_{3g}	5.89	5.93	5.52	6.17	5.07	4.94
c^1A_g	5.99	6.03	5.54	6.44	5.09	
b^1B_{1u}	5.61 (1.024)	5.65 (1.041)	5.32 (0.791)	5.77 (1.154)	5.28 (1.29)	5.15-5.40

Rydberg states

State	CAM-B3LYP DunRy	M06-2X DunRy	B3LYP DunRy	wB97X DunRy	RASPT2 ANO-RCC[c]
a^1B_{1g} (Rs)	5.11	5.02	4.70	5.66	5.05
a^1B_{3u} (Rpy)	5.39	5.27	4.95	6.00 (10^{-3})	5.44
a^1A_u (Rpz)	5.43	5.30	4.92	6.07	5.41
c^1B_{2u} (Rpx)	5.69 (10^{-3})	5.57 (10^{-3})	5.30	6.16	
b^1B_{1g} (Rd)	5.81	5.68	5.28	6.34	
a^1B_{2g} (Rd)	5.83	5.68	5.33	6.43	

[a]Refs [53–59]

[b]ANO-RCC basis set [4s3p2d] for C and [2s1p] for H. CAS(16,16) with all π orbitals[30]

[c]ANO-RCC basis set [3s2p1d]/[2s1p] for C/H and Ry basis set at the center of charge of the cation. RAS2(16,16) with all π and RAS3 with one Rydberg orbital

Pure $n_O \rightarrow \pi^\star$ states are not present when there is only one water molecule while the excitation energies of these $n_O \rightarrow \pi^\star$ states appear slightly below 6 eV only for the 2-cav and 2-side configurations. For the $C_{20}H_{10}(H_2O)_3$ stoichiometry, the $n_O \rightarrow \pi^\star$ states are found above 6 eV in the case of the 3-cav configuration. In the other cases, these excitations are mixed with $\pi \rightarrow \pi^\star$ ones.

Interestingly, as can be seen in Tables 3 to 5, the interaction with water molecules leads to an increase of the VIP except in the case of the 1-side isomer. This increase correlates with a larger Nb(H–C) and smaller Nb(O–H).

Table 2 Bare corannulene: effect of the DFT functional on the excitation energies. D stands for "diffuse orbitals" that can be Rydberg orbitals, SAMOs or mixed.

CAM-B3LYP		M06-2X		B3LYP		wB97X		Exp[a]
$\pi \rightarrow \pi^\star$	3.83	$\pi \rightarrow \pi^\star$	3.83	$\pi \rightarrow \pi^\star$	3.47	$\pi \rightarrow \pi^\star$	4.03	
$\pi \rightarrow \pi^\star$	3.86	$\pi \rightarrow \pi^\star$	3.88	$\pi \rightarrow \pi^\star$	3.50	$\pi \rightarrow \pi^\star$	4.03	
$\pi \rightarrow \pi^\star$	3.86	$\pi \rightarrow \pi^\star$	3.88	$\pi \rightarrow \pi^\star$	3.50	$\pi \rightarrow \pi^\star$	4.04	
$\pi \rightarrow \pi^\star$	4.12	$\pi \rightarrow \pi^\star$	4.17	$\pi \rightarrow \pi^\star$	3.75	$\pi \rightarrow \pi^\star$	4.32	
$\pi \rightarrow \pi^\star$	4.12	$\pi \rightarrow \pi^\star$	4.17	$\pi \rightarrow \pi^\star$	3.75	$\pi \rightarrow \pi^\star$	4.32	
$\pi \rightarrow \pi^\star$	4.55 (0.02)	$\pi \rightarrow \pi^\star$	4.54 (0.02)	$\pi \rightarrow \pi^\star$	3.97 (0.01)	$\pi \rightarrow \pi^\star$	4.88 (0.03)	3.71
$\pi \rightarrow \pi^\star$	4.81 (0.44)	$\pi \rightarrow \pi^\star$	4.81 (0.43)	$\pi \rightarrow \pi^\star$	4.27 (0.24)	$\pi \rightarrow \pi^\star$	5.11 (0.59)	4.36
$\pi \rightarrow \pi^\star$	4.81 (0.44)	$\pi \rightarrow \pi^\star$	4.81 (0.43)	$\pi \rightarrow \pi^\star$	4.27 (0.25)	$\pi \rightarrow \pi^\star$	5.11 (0.69)	4.36
$\pi \rightarrow \pi^\star$	5.53 (0.49)	$\pi \rightarrow \pi^\star$	5.54 (0.48)	$\pi \rightarrow \pi^\star$	5.12 (0.31)	$\pi \rightarrow \pi^\star$	5.76 (0.53)	4.97
$\pi \rightarrow \pi^\star$	5.54 (0.49)	$\pi \rightarrow \pi^\star$	5.54 (0.48)	$\pi \rightarrow \pi^\star$	5.12 (0.30)	$\pi \rightarrow \pi^\star$	5.76 (0.53)	4.97
$\pi \rightarrow \pi^\star$/D	5.79	$\pi \rightarrow$ D	5.81	$\pi \rightarrow \pi^\star$	5.23	$\pi \rightarrow \pi^\star$	6.19	
$\pi \rightarrow \pi^\star$/D	5.79	$\pi \rightarrow$ D	5.81	$\pi \rightarrow \pi^\star$	5.23	$\pi \rightarrow \pi^\star$	6.20	
$\pi \rightarrow$ D	5.91	$\pi \rightarrow \pi^\star$/D	5.90	$\pi \rightarrow$ D	5.37			
$\pi \rightarrow$ D	5.91	$\pi \rightarrow \pi^\star$/D	5.90	$\pi \rightarrow$ D	5.38			
$\pi \rightarrow \pi^\star$/D	5.94	$\pi \rightarrow$ D (p)	6.02	$\pi \rightarrow$ D	5.48			
$\pi \rightarrow \pi^\star$	6.10 (0.01)	$\pi \rightarrow \pi^\star$	6.11	$\pi \rightarrow$ D	5.49			
$\pi \rightarrow \pi^\star$	6.10 (0.01)	$\pi \rightarrow \pi^\star$	6.11	$\pi \rightarrow \pi^\star$	5.53			

[a] ref [60]

In the case of the 1-side isomer, there is one Nb(O–H) for zero Nb(H–C), which is in line with a decrease of the VIP. There is then a correlation between the orientation of the closest water molecules to corannulene and the VIP variation with respect to bare corannulene: a large Nb(O–H) favors a decrease of the VIP, a large Nb(H–C) favors an increase of the VIP.

3.3 Results for pyrene

The nature and the energies of the transitions up to $\sim$6 eV for bare $C_{16}H_{10}$ and $(C_{16}H_{10})(H_2O)_n$ are reported in Tables 6, 7 and 8 for n=1,2 and 3 respectively. Some representative NTOs are also reported in Fig. 7.

As can be seen in the first column of Tables 6 to 8, the first five transitions for $C_{16}H_{10}$ are $\pi \rightarrow \pi^\star$ transitions, followed by a $\pi \rightarrow$Rs transition at 5.11 eV. Focusing first on the model systems (n=1), upon interaction with one water molecule whatever the conformation ("side" GEO1_IP$_{Min}$ or "face" GEO1_IP$_{Max}$),

Table 3 Corannulene + H_2O. TD-DFT CAM-B3LYP excitation energies (eV) and, in parenthesis, oscillator strengths. Excitations with small contributions are given in parenthesis. The VIP values (in eV) and the number of bonds shorter than 3Å between the H (resp. O) atoms of the water molecules and the C (resp. H) atoms of corannulene (Nb(H–C) (resp. Nb(O–H)) are also reported. D stands for "diffuse orbitals" that can be Rydberg orbitals, SAMOs or mixed.

Bare		1-vex		1-cav		1-side	
$\pi\rightarrow\pi^\star$	3.83	$\pi\rightarrow\pi^\star$	3.84	$\pi\rightarrow\pi^\star$	3.86	$\pi\rightarrow\pi^\star$	3.81
$\pi\rightarrow\pi^\star$	3.86	$\pi\rightarrow\pi^\star$	3.86	$\pi\rightarrow\pi^\star$	3.88	$\pi\rightarrow\pi^\star$	3.83
$\pi\rightarrow\pi^\star$	3.86	$\pi\rightarrow\pi^\star$	3.88	$\pi\rightarrow\pi^\star$	3.89	$\pi\rightarrow\pi^\star$	3.85
$\pi\rightarrow\pi^\star$	4.12	$\pi\rightarrow\pi^\star$	4.10	$\pi\rightarrow\pi^\star$	4.13	$\pi\rightarrow\pi^\star$	4.11
$\pi\rightarrow\pi^\star$	4.12	$\pi\rightarrow\pi^\star$	4.14	$\pi\rightarrow\pi^\star$	4.13	$\pi\rightarrow\pi^\star$	4.14
$\pi\rightarrow\pi^\star$	4.55 (0.02)	$\pi\rightarrow\pi^\star$	4.54 (0.03)	$\pi\rightarrow\pi^\star$	4.56 (0.02)	$\pi\rightarrow\pi^\star$	4.52 (0.02)
$\pi\rightarrow\pi^\star$	4.81 (0.44)	$\pi\rightarrow\pi^\star$	4.82 (0.44)	$\pi\rightarrow\pi^\star$	4.82 (0.45)	$\pi\rightarrow\pi^\star$	4.82 (0.45)
$\pi\rightarrow\pi^\star$	4.81 (0.44)	$\pi\rightarrow\pi^\star$	4.82 (0.46)	$\pi\rightarrow\pi^\star$	4.82 (0.44)	$\pi\rightarrow\pi^\star$	4.82 (0.46)
$\pi\rightarrow\pi^\star$	5.53 (0.49)	$\pi\rightarrow\pi^\star$	5.56 (0.47)	$\pi\rightarrow\pi^\star$ (D)	5.53 (0.47)	$\pi\rightarrow\pi^\star$ (D)	5.50 (0.40)
$\pi\rightarrow\pi^\star$	5.54 (0.49)	$\pi\rightarrow\pi^\star$	5.56 (0.44)	$\pi\rightarrow\pi^\star$ (D)	5.57 (0.47)	$\pi\rightarrow\pi^\star$ (D)	5.53 (0.43)
$\pi\rightarrow\pi^\star$/D	5.79	$\pi\rightarrow\pi^\star$(D)	5.82	$\pi\rightarrow\pi^\star$/D	5.81	$\pi\rightarrow$D ($\pi^\star$)	5.64 (0.10)
$\pi\rightarrow\pi^\star$/D	5.79	$\pi\rightarrow\pi^\star$(D)	5.84	$\pi\rightarrow\pi^\star$/D	5.82	$\pi\rightarrow$D ($\pi^\star$)	5.72 (0.03)
$\pi\rightarrow$D	5.91 (0.02)	$\pi\rightarrow$D	6.00 ($3{\cdot}10^{-3}$)	$\pi\rightarrow$D/$\pi^\star$	6.05	$\pi\rightarrow$Rs ($\pi^\star$)	5.79 (0.02)
$\pi\rightarrow$D	5.91 (0.02)	$\pi\rightarrow$D	6.01	$\pi\rightarrow$D/$\pi^\star$	6.07	$\pi\rightarrow$Rs/$\pi^\star$	5.81 (0.03)
$\pi\rightarrow$D/$\pi^\star$	5.94	$\pi\rightarrow$D	6.03 ($2{\cdot}10^{-3}$)	$\pi\rightarrow$D	6.11	$\pi\rightarrow\pi^\star$ (Rs)	5.89 (0.01)
$\pi\rightarrow$D/$\pi^\star$	5.94	$\pi\rightarrow$D	6.03 ($3{\cdot}10^{-3}$)	$\pi\rightarrow$D (Rp)	6.11	$\pi\rightarrow\pi^\star$ (Rs)	5.91
$\pi\rightarrow\pi^\star$	6.10 (0.01)	$\pi\rightarrow\pi^\star$	6.08 (0.03)	$\pi\rightarrow\pi^\star$	6.15 (0.03)	$\pi\rightarrow$Rs/Rp	5.95 (0.01)
$\pi\rightarrow\pi^\star$	6.10 (0.01)	$\pi\rightarrow\pi^\star$	6.08 (0.03)	$\pi\rightarrow\pi^\star$	6.17 (0.02)	$\pi\rightarrow$D (Rs)	5.99
						$\pi\rightarrow$D (Rs)	6.04 ($2{\cdot}10^{-3}$)
VIP	7.98		8.19		8.17		7.75
Nb(H–C)			6		11		0
Nb(O–H)			0		0		1

the Rydberg s (Rs) target orbital becomes mixed with a diffuse molecular orbital developed mainly on the non-interacting hydrogen atoms of the water molecules (/wat) (see Table 6). Such virtual orbital involved in the NTOs is named wat/Rs or Rs/wat orbital in the tables depending on the respective weight of the diffuse/Rydberg orbitals. This leads to two $\pi\rightarrow$wat/Rs transitions at 4.80 and 5.06 eV for GEO1_IP$_{Min}$, the NTOs corresponding to the lowest energy one are reported in Fig. 7. Interestingly, the lowest energy transition of this type (4.80 eV) is lower in energy than the third $\pi\rightarrow\pi^\star$ transitions and than all other $\pi\rightarrow$R transitions as well. In the case of GEO1_IP$_{Max}$, such transition is not observed, but the lowest $\pi\rightarrow$Rs/wat excitation, that is to say where the target orbital involves water but has mostly a Rydberg character, is found at 5.22 eV. A similar transition is found at lower energy (5.06 eV) in the case of GEO1_IP$_{Min}$. The NTOs for these transitions are also reported in Fig. 7. The $\pi\rightarrow$wat/Rs transitions at 4.80 eV can be regarded as a PAH^+-H_2O^- CT state. However, it has a null oscillator strength and therefore can not explain the photo-reactivity observed in the noble gas matrix [13]. The en-

Table 4 Corannulene + 2 H_2O. TD-DFT CAM-B3LYP excitation energies (eV) and, in parenthesis, oscillator strengths. Excitations with small contributions are given in parenthesis. The VIP values (in eV) and the number of bonds shorter than 3Å between the H (resp. O) atoms of the water molecules and the C (resp. H) atoms of corannulene (Nb(H–C) (resp. Nb(O–H)) are also reported. D stands for "diffuse orbitals" that can be Rydberg orbitals, SAMOs or mixed.

Bare		2-vex		2-cav		2-vex-side		2-cav-side	
$\pi\rightarrow\pi^\star$	3.83	$\pi\rightarrow\pi^\star$	3.79	$\pi\rightarrow\pi^\star$	3.86	$\pi\rightarrow\pi^\star$	3.84	$\pi\rightarrow\pi^\star$	3.87
$\pi\rightarrow\pi^\star$	3.86	$\pi\rightarrow\pi^\star$	3.86 (10^{-3})	$\pi\rightarrow\pi^\star$	3.86	$\pi\rightarrow\pi^\star$	3.86	$\pi\rightarrow\pi^\star$	3.88 (10^{-3})
$\pi\rightarrow\pi^\star$	3.86	$\pi\rightarrow\pi^\star$	3.94 (10^{-3})	$\pi\rightarrow\pi^\star$	3.89	$\pi\rightarrow\pi^\star$	3.88	$\pi\rightarrow\pi^\star$	3.89
$\pi\rightarrow\pi^\star$	4.12	$\pi\rightarrow\pi^\star$	4.09	$\pi\rightarrow\pi^\star$	4.12	$\pi\rightarrow\pi^\star$	4.11	$\pi\rightarrow\pi^\star$	4.12 (10^{-3})
$\pi\rightarrow\pi^\star$	4.12	$\pi\rightarrow\pi^\star$	4.13	$\pi\rightarrow\pi^\star$	4.16 (10^{-3})	$\pi\rightarrow\pi^\star$	4.12	$\pi\rightarrow\pi^\star$	4.15
$\pi\rightarrow\pi^\star$	4.55 (0.02)	$\pi\rightarrow\pi^\star$	4.53 (0.04)	$\pi\rightarrow\pi^\star$	4.56 (0.02)	$\pi\rightarrow\pi^\star$	4.54 (0.02)	$\pi\rightarrow\pi^\star$	4.56 (0.02)
$\pi\rightarrow\pi^\star$	4.81 (0.44)	$\pi\rightarrow\pi^\star$	4.80 (0.44)	$\pi\rightarrow\pi^\star$	4.82 (0.42)	$\pi\rightarrow\pi^\star$	4.80 (0.43)	$\pi\rightarrow\pi^\star$	4.82 (0.44)
$\pi\rightarrow\pi^\star$	4.81 (0.44)	$\pi\rightarrow\pi^\star$	4.81 (0.48)	$\pi\rightarrow\pi^\star$	4.82 (0.43)	$\pi\rightarrow\pi^\star$	4.80 (0.49)	$\pi\rightarrow\pi^\star$	4.82 (0.44)
$\pi\rightarrow\pi^\star$	5.53 (0.49)	$\pi\rightarrow\pi^\star$	5.54 (0.47)	$\pi\rightarrow\pi^\star$(D)	5.53 (0.45)	$\pi\rightarrow\pi^\star$ (D)	5.48 (0.40)	$\pi\rightarrow\pi^\star$ (D)	5.52 (0.45)
$\pi\rightarrow\pi^\star$	5.54 (0.49)	$\pi\rightarrow\pi^\star$	5.59 (0.38)	$\pi\rightarrow\pi^\star$(D)	5.57 (0.47)	$\pi\rightarrow\pi^\star$ (D)	5.50 (0.43)	$\pi\rightarrow\pi^\star$ (D)	5.56 (0.45)
$\pi\rightarrow\pi^\star$/D	5.79	$\pi\rightarrow\pi^\star$	5.81 (0.01)	$\pi\rightarrow\pi^\star$(D)	5.82	$\pi\rightarrow\pi^\star$/D	5.75 ($4{\cdot}10^{-3}$)	$\pi\rightarrow\pi^\star$/D	5.78 ($3{\cdot}10^{-3}$)
$\pi\rightarrow\pi^\star$/D	5.79	$\pi\rightarrow\pi^\star$ $n_O\rightarrow\pi^\star$	5.83 (0.001)	$\pi\rightarrow\pi^\star$(D)	5.85 (10^{-3})	$\pi\rightarrow\pi^\star$/D	5.75 (0.02)	$\pi\rightarrow\pi^\star$/D	5.82 (10^{-3})
$\pi\rightarrow$D	5.91 (0.02)	$n_O\rightarrow\pi^\star$	5.84 (10^{-3})	$n_O\rightarrow\pi^\star$	5.85 (6.10−3)	$\pi\rightarrow D/\pi^\star$	5.91	$\pi\rightarrow$D/$\pi^\star$	6.00
$\pi\rightarrow$D	5.91 (0.02)	$n_O\rightarrow\pi^\star$	5.95 ($2{\cdot}10^{-3}$)	$n_O\rightarrow\pi^\star$	5.95 (10^{-3})	$\pi\rightarrow$D/$\pi^\star$	5.92 (0.04)	$\pi\rightarrow$D/$\pi^\star$	6.02 ($3{\cdot}10^{-3}$)
$\pi\rightarrow$D/$\pi^\star$	5.94	$\pi\rightarrow$D	6.01 ($5{\cdot}10^{-3}$)	$\pi\rightarrow$D $\pi\rightarrow\pi^\star$ $n_O\rightarrow\pi^\star$	6.11 ($5{\cdot}10^{-3}$)	$\pi\rightarrow\pi^\star$/D/Rp	5.97 (10^{-3})	$\pi\rightarrow$D/$\pi^\star$	6.04 ($3{\cdot}10^{-3}$)
$\pi\rightarrow$D/$\pi^\star$	5.94	$\pi\rightarrow$D/$\pi^\star$	6.03 (0.01)	$\pi\rightarrow$D $\pi\rightarrow\pi^\star$ $n_O\rightarrow\pi^\star$	6.11 ($5{\cdot}10^{-3}$)	$\pi\rightarrow$D/$\pi^\star$	5.99 (10^{-3})	$\pi\rightarrow$D/$\pi^\star$	6.06 ($4{\cdot}10^{-3}$)
$\pi\rightarrow\pi^\star$	6.10 (0.01)	$\pi\rightarrow\pi^\star$/D	6.05 (0.03)	$\pi\rightarrow$D	6.20 ($3{\cdot}10^{-3}$)	$\pi\rightarrow$D/$\pi^\star$	5.99 (10^{-3})	$n_O\rightarrow\pi^\star$ $\pi\rightarrow\pi^\star$	6.09 (0.03)
$\pi\rightarrow\pi^\star$	6.10 (0.01)	$\pi\rightarrow$D	6.08 ($3{\cdot}10^{-3}$)	$\pi\rightarrow$D	6.21 ($7{\cdot}10^{-3}$)	$\pi\rightarrow\pi^\star$ $n_O\rightarrow\pi^\star$	6.09 (0.01)	$n_O\rightarrow\pi^\star$ $\pi\rightarrow\pi^\star$	6.14 (0.02)
VIP	7.98		8.30		8.36		8.05		8.16
Nb(H–C)			8		15		6		15
Nb(O–H)			0		0		2		2

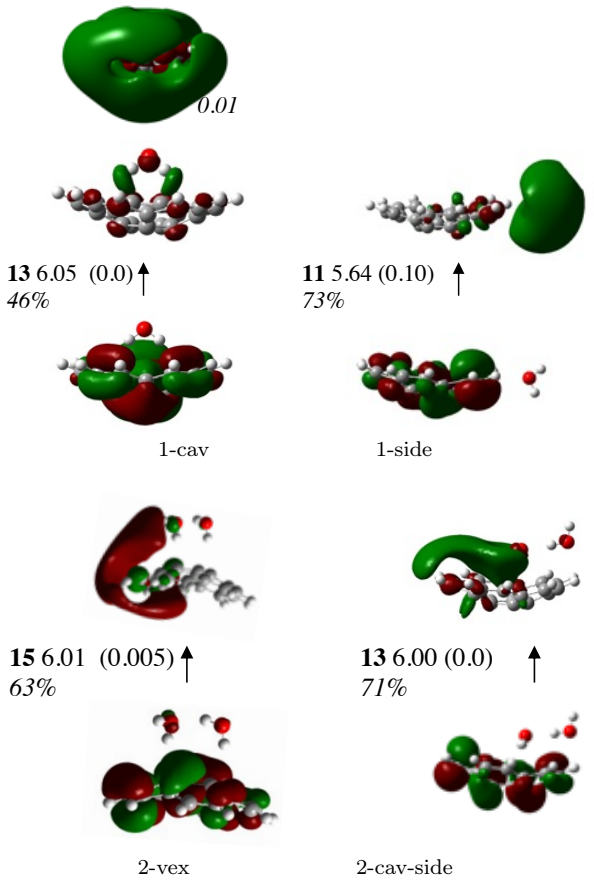

Fig. 6 Examples of NTOs for $(C_{20}H_{10})(H_2O)_n$ isomers, n=1,2 from top to bottom. Unless specified, an isovalue of 0.02 was used for both hole and particle orbitals.

vironment is likely to play a role on the oscillator strength for such transition, as will be detailed in the following.

Concerning $(C_{16}H_{10})(H_2O)_n$ with n≥2, the NTOs show that the holes are mainly created in π orbitals but are slightly developed on the n_O orbitals of the oxygen atoms of the water molecules pointing towards the PAH (this is reminded quoting $(+n_O)$ in the first line of the tables). This contribution is therefore more noticeable (but remains small) for the GEOn_IP_{Max} series. As in the case of the model systems (n=1), the Rs orbital becomes mixed with a diffuse molecular orbital developed mainly on the non-interacting hydrogen atoms of the water molecules (Rs/wat) for n=2 and 3 and for all clusters, and there is a low energy $\pi \rightarrow$Rs/wat transition. In the case of GEOn_IP_{Min} (n=2,3), the lowest energy transition of this type is found at 5.11 eV for n=2 and decreases to 4.93 eV for n=3. Interestingly, the oscillator strength of such

Table 5 Corannulene + 3 H_2O. TD-DFT CAM-B3LYP excitation energies (eV) and, in parenthesis, oscillator strengths . Excitations with small contributions are given in parenthesis. The VIP values (in eV) and the number of bonds shorter than 3Å between the H (resp. O) atoms of the water molecules and the C (resp. H) atoms of corannulene (Nb(H–C) (resp. Nb(O–H)) are also reported. D stands for "diffuse orbitals" that can be Rydberg orbitals or SAMOs or mixed.

Bare		3-vex		3-cav		3-vex-side		3-cav-side	
$\pi\rightarrow\pi^\star$	3.83	$\pi\rightarrow\pi^\star$	3.82	$\pi\rightarrow\pi^\star$	3.79	$\pi\rightarrow\pi^\star$	3.79	$\pi\rightarrow\pi^\star$	3.81
$\pi\rightarrow\pi^\star$	3.86	$\pi\rightarrow\pi^\star$	3.85	$\pi\rightarrow\pi^\star$	3.83	$\pi\rightarrow\pi^\star$	3.86	$\pi\rightarrow\pi^\star$	3.84
$\pi\rightarrow\pi^\star$	3.86	$\pi\rightarrow\pi^\star$	3.91	$\pi\rightarrow\pi^\star$	3.85	$\pi\rightarrow\pi^\star$	3.92	$\pi\rightarrow\pi^\star$	3.87
$\pi\rightarrow\pi^\star$	4.12	$\pi\rightarrow\pi^\star$	4.10	$\pi\rightarrow\pi^\star$	4.13 ($2{\cdot}10^{-3}$)	$\pi\rightarrow\pi^\star$	4.09	$\pi\rightarrow\pi^\star$	4.12 (10^{-3})
$\pi\rightarrow\pi^\star$	4.12	$\pi\rightarrow\pi^\star$	4.15	$\pi\rightarrow\pi^\star$	4.13	$\pi\rightarrow\pi^\star$	4.12	$\pi\rightarrow\pi^\star$	4.15 (10^{-3})
$\pi\rightarrow\pi^\star$	4.55 (0.02)	$\pi\rightarrow\pi^\star$	4.53 (0.04)	$\pi\rightarrow\pi^\star$	4.52 (0.02)	$\pi\rightarrow\pi^\star$	4.52 (0.02)	$\pi\rightarrow\pi^\star$	4.53 (0.02)
$\pi\rightarrow\pi^\star$	4.81 (0.44)	$\pi\rightarrow\pi^\star$	4.83 (0.44)	$\pi\rightarrow\pi^\star$	4.81 (0.41)	$\pi\rightarrow\pi^\star$	4.80 (0.46)	$\pi\rightarrow\pi^\star$	4.81 (0.42)
$\pi\rightarrow\pi^\star$	4.81 (0.44)	$\pi\rightarrow\pi^\star$	4.83 (0.46)	$\pi\rightarrow\pi^\star$	4.82 (0.42)	$\pi\rightarrow\pi^\star$	4.80 (0.50)	$\pi\rightarrow\pi^\star$	4.82 (0.47)
$\pi\rightarrow\pi^\star$	5.53 (0.49)	$\pi\rightarrow\pi^\star$	5.57 (0.47)	$\pi\rightarrow\pi^\star$(D)	5.53 (0.45)	$\pi\rightarrow\pi^\star$ (D)	5.50 (0.39)	$\pi\rightarrow\pi^\star$	5.53 (0.47)
$\pi\rightarrow\pi^\star$	5.54 (0.49)	$\pi\rightarrow\pi^\star$	5.60 (0.43)	$\pi\rightarrow\pi^\star$(D)	5.57 (0.46)	$\pi\rightarrow\pi^\star$ (D)	5.54 (0.38)	$\pi\rightarrow\pi^\star$	5.55 (0.51)
$\pi\rightarrow\pi^\star$/D	5.79	$\pi\rightarrow\pi^\star$	5.85	$\pi\rightarrow\pi^\star$(D)	5.87	$\pi\rightarrow\pi^\star$/D	5.78 (0.02)	$\pi\rightarrow$D/$\pi^\star$	5.83 ($5{\cdot}10^{-3}$)
$\pi\rightarrow\pi^\star$/D	5.79	$\pi\rightarrow\pi^\star$	5.87 (10^{-3})	$\pi\rightarrow\pi^\star$(D)	5.90	$\pi\rightarrow\pi^\star$/D	5.80 ($3{\cdot}10^{-3}$)	$\pi\rightarrow$D/$\pi^\star$	5.84 ($2{\cdot}10^{-3}$)
$\pi\rightarrow$D	5.91 (0.02)	$\pi\rightarrow$D	6.02	$n_O\rightarrow\pi^\star$ $\pi\rightarrow\pi^\star$	6.12 ($6{\cdot}10^{-3}$)	$\pi\rightarrow D/\pi^\star$	5.89 (0.04)	$\pi\rightarrow$D/$\pi^\star$	5.85 ($6{\cdot}10^{-3}$)
$\pi\rightarrow$D	5.91 (0.02)	$\pi\rightarrow$D	6.03 (10^{-3})	$n_O\rightarrow\pi^\star$ $\pi\rightarrow\pi^\star$	6.13 ($4{\cdot}10^{-3}$)	$\pi\rightarrow$D/$\pi^\star$	5.94 (0.03)	$\pi\rightarrow\pi^\star$/D	5.87
$\pi\rightarrow\pi^\star$/D	5.94	$\pi\rightarrow$D	6.05 ($4{\cdot}10^{-3}$)	$n_O\rightarrow\pi^\star$	6.24	$\pi\rightarrow\pi^\star$/D	5.98	$\pi\rightarrow$D/$\pi^\star$	5.92 ($4{\cdot}10^{-3}$)
$\pi\rightarrow\pi^\star$/D	5.94	$\pi\rightarrow$D	6.06 ($5{\cdot}10^{-3}$)	$n_O\rightarrow\pi^\star$ $\pi\rightarrow\pi^\star$ $\pi\rightarrow$D	6.25 ($2{\cdot}10^{-3}$)	$\pi\rightarrow\pi^\star$/D	6.00	$\pi\rightarrow$D/$\pi^\star$	5.94 ($3{\cdot}10^{-3}$)
$\pi\rightarrow\pi^\star$	6.10 (0.01)	$\pi\rightarrow\pi^\star$	6.08 (0.03)	$\pi\rightarrow\pi^\star$ $n_O\rightarrow\pi^\star$	6.26 (10^{-3})	$\pi\rightarrow\pi^\star$ $n_O\rightarrow\pi^\star$	6.08 (0.03)	$\pi\rightarrow\pi^\star$ $n_O\rightarrow\pi^\star$	6.12 ($7{\cdot}10^{-3}$)
$\pi\rightarrow\pi^\star$	6.10 (0.01)	$\pi\rightarrow\pi^\star$	6.11 (0.03)	$n_O\rightarrow\pi^\star$	6.27 (10^{-3})	$\pi\rightarrow\pi^\star$ $n_O\rightarrow\pi^\star$	6.10 (0.02)	$\pi\rightarrow\pi^\star$ $n_O\rightarrow\pi^\star$	6.13 (10^{-3})
VIP	7.98		8.18		8.42		8.02		8.08
Nb(H–C)			8		11		3		6
Nb(O–H)			0		0		1		2

transition increases with the number of water molecules ($3{\cdot}10^{-3}$ for n=2 and 9.10^{-2} for n=3). The NTOs for these transitions are reported in Fig. 7 as NTOs 6 and 4 for n=2 and 3 respectively. In the case of GEO2_IP$_{Min}$, low energy transitions from π orbitals to mixed Rpy/wat/$\pi^\star$ are also observed at 5.38 and 5.46 eV with small oscillator strength also ($2{\cdot}10^{-3}$ and $5{\cdot}10^{-3}$ respectively). Regarding GEO3_IP$_{Min}$, two other $\pi\rightarrow$R/wat transitions are found at 5.33 and 5.37 eV with an oscillator strength of 10^{-3} (see Fig. 7 NTO

8 for instance). Interestingly, the lowest energy $\pi \rightarrow$Rs/wat transition of the GEOn_IP$_{Max}$ isomer is systematically higher in energy and with a lower oscillator strength than that of the corresponding GEOn_IP$_{Min}$ isomer.
From these results, the configurations of the GEOn_IP$_{Min}$ with at least one water molecule having its oxygen atom close to a hydrogen atom of pyrene, are expected to favor the formation of a PAH^+-H_2O^- CT state all the more as the number of water molecules increases.

Regarding the higher energy transitions not relevant to interpret the photoreactivity, the interaction with water molecules modifies the energies of the other $\pi \rightarrow \pi^\star$ and $\pi \rightarrow$R transitions. In the electronic spectrum of bare pyrene, $\pi \rightarrow$Rp transitions are found at higher energies (5.39, 5.42 and 5.69 eV). When n=1, these transitions, similar to those involving the Rs orbitals, are lower in energy for GEO1_IP$_{Min}$ and higher in energy for GEO1_IP$_{Max}$. The transitions towards the Rd Rydberg orbitals, higher in energy, follow the same trends: they are lower in energy for GEO1_IP$_{Min}$ and higher in energy for GEO1_IP$_{Max}$. When the number of water molecules increases, the Rp Rydberg obitals mix with $\pi^\star$ orbitals in the case of both GEOn_IP$_{Min}$ and GEOn_IP$_{Max}$ series, and with diffuse orbitals located on the H atoms of the water molecules in the case of the GEOn_IP$_{Min}$ systems.
Globally, the energies of the transitions towards the orbitals mainly of Rp and Rd nature tend to decrease in the GEOn_IP$_{Min}$ systems although it is not observed for n=2 and tend to increase for the GEOn_IP$_{Max}$ series. The oscillator strengths of these transitions tend to increase upon interaction with the water molecules.
Regarding $\pi \rightarrow \pi^\star$ transitions that remain pure upon interaction with water molecules, they are slightly affected.

In order to study the influence of the number of water molecules on the electronic spectrum of pyrene and hence to investigate the trends when going from a small number of water molecules to a cluster that can be considered as a first shell of Ih ice, the electronic states for GEO16_IP$_{Min}$ and GEO15_IP$_{Max}$ - size of the solvation sphere of 3.82 Å - were computed and analysed (see Table 9). Interestingly, increasing the number of water molecules leads to several occurrences of low energy transitions involving $\pi \rightarrow$R/wat excitations for GEO16_IP$_{Min}$. The diffuse orbitals /wat are mainly developed on the free hydrogen atoms (also called "dangling" H for ice) for the most external water molecules. This is very similar to what was found for benzene-water complexes [26]. Furthermore, one transition found for GEO16_IP$_{Min}$ at 5.40 eV from a mixed π/n_O to a diffuse orbital /wat corresponds to the first excited state of $(H_2O)_{16}$ (5.42 eV) in the same geometry (see Figure 8). In the case of benzene-water clusters, these excitations were more numerous as more states were investigated. Interestingly, the water cluster excess electron occupying such diffuse /wat orbital is in line with the cavity model used to described the excess electron in liquid water [67]. In GEO16_IP$_{Min}$, the oscillator strengths

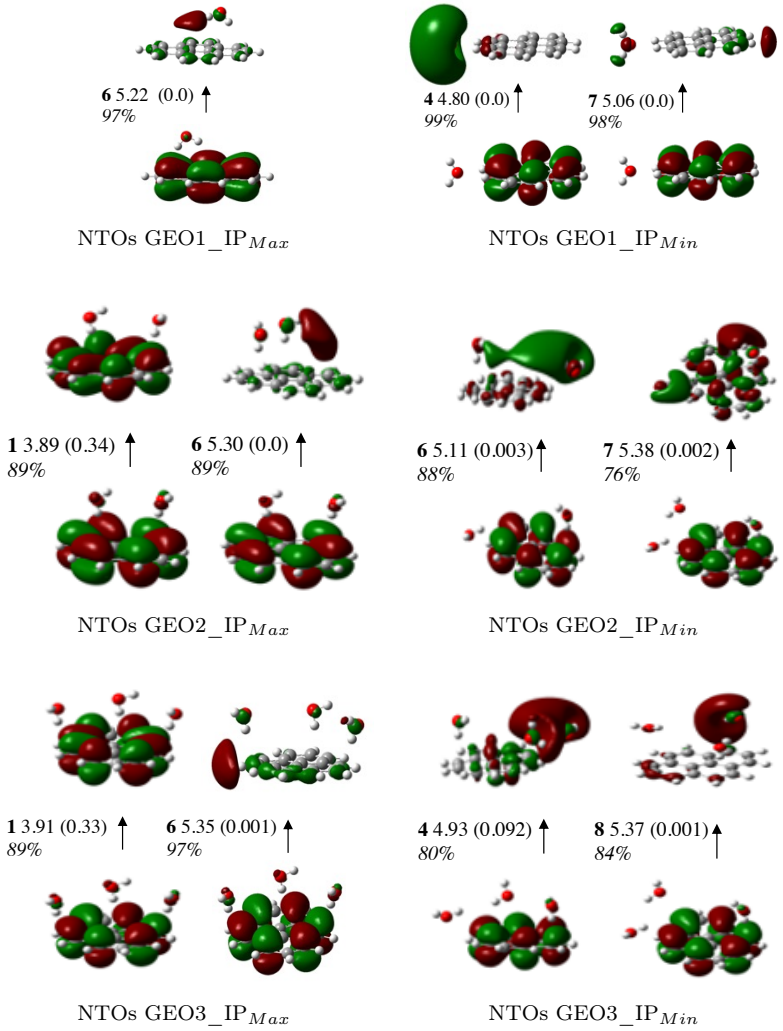

Fig. 7 Examples of NTOs for $(C_{16}H_{10})(H_2O)_n$ isomers, n=1-3 from top to bottom. An isovalue of 0.02 was used for both hole and particle orbitals.

of $\pi \rightarrow$R/wat excitations are small (see NTO 3 on top of Fig. 9). When mixing with $\pi \rightarrow \pi^\star$ excitations, the oscillator strength increases (see NTO 6 on top of Fig. 9 and the two main excitations for transition 7 (NTO 7)). In the case of GEO15_IP$_{Max}$, the multi-determinantal character of the low energy transitions was found to be enhanced with respect to GEO16_IP$_{Min}$. The first lowest energy transition involving a $\pi \rightarrow$R/wat excitation was found at 5.45 eV (see NTO 6 at the bottom of Fig. 9). Globally, much fewer low energy transitions involving $\pi \rightarrow$R/wat excitations than for GEO16_IP$_{Min}$ were found and

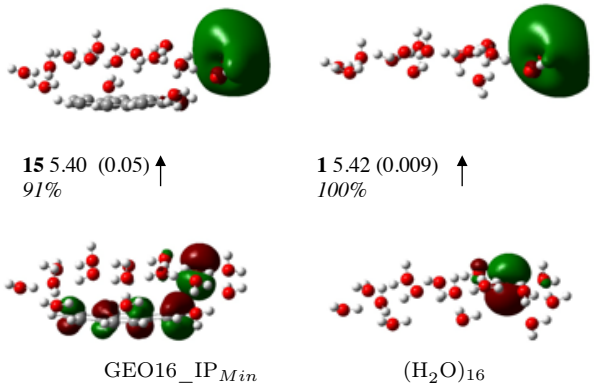

Fig. 8 Left: NTO corresponding to 15^{th} transition for GEO16_IP$_{Min}$; right: corresponding NTO for the bare water cluster at the same geometry. An isovalue of 0.02 was used for both hole and particle orbitals.

all with small oscillator strength.

Pure $n_O \rightarrow \pi^\star$ transitions are found for GEO15_IP$_{Max}$, occurring above 6.00 eV. They are neither found for GEO16_IP$_{Min}$ nor for a smaller number of water molecules in the case of pyrene, contrary to corannulene.

Globally, the presence of low energy $\pi \rightarrow$R/wat transitions is in line with low vertical ionisation energies. As in the case of corannulene, a correlation was established between a large Nb(C–H) value and an increase of the VIP with respect to that of bare pyrene. On the opposite, a large number of Nb(O–H) is in favor of a decrease of the VIP. It is clear for n=1 and for n=15,16. For the intermediate numbers of water molecules (n=2,3) and the GEOn_IP$_{Min}$ series, there are more Nb(C–H) than Nb(O–H) and the VIP remains higher than that of bare pyrene.

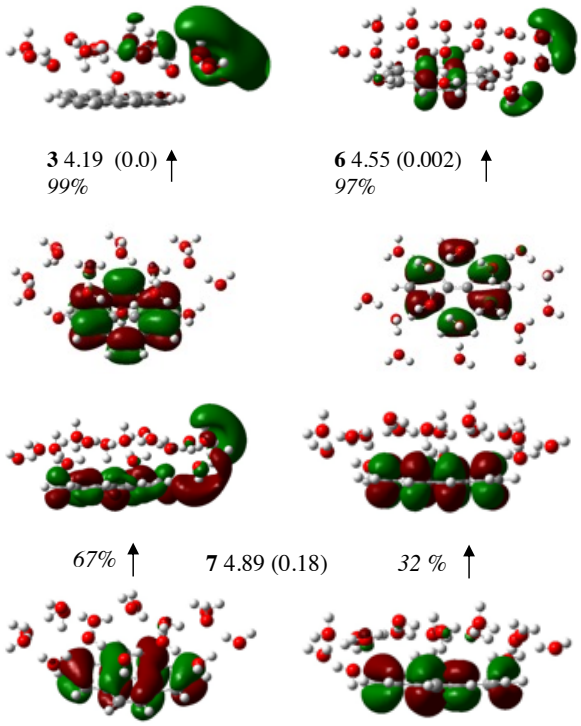

NTOs GEO16_IP$_{Min}$

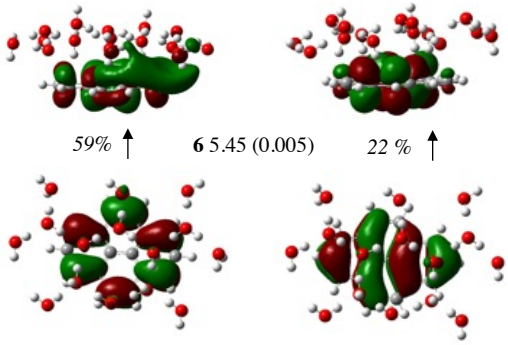

NTO GEO15_IP$_{Max}$

Fig. 9 Examples of NTOs for $C_{16}H_{10}(H_2O)_n$ (n=15,16): three are reported for GEO16_IP$_{Min}$ (top) and one GEO15_IP$_{Max}$ (bottom). An isovalue of 0.02 was used for both hole and particle orbitals.

Table 6 Pyrene + H_2O. TD-DFT CAM-B3LYP excitation energies (eV) and, in parenthesis, oscillator strengths. Excitations with small contributions are given in parenthesis. /wat means that the MO also involves H and, to lesser extent, O diffuse atomic orbitals of the water molecules. The VIP values (in eV) and the number of bonds shorter than 3Å between the H (resp. O) atoms of the water molecules and the C (resp. H) atoms of pyrene (Nb(H–C) (resp. Nb(O–H)) are also reported. R stands for "Rydberg orbitals". The transitions to states developed on both /wat and Rydberg orbitals are reported in bold characters.

Bare		GEO1_IP$_{Min}$ (side)		GEO1_IP$_{Max}$ (face)	
$\pi\rightarrow\pi^\star$	3.92	$\pi\rightarrow\pi^\star$	3.91 (0.30)	$\pi\rightarrow\pi^\star$	3.91 (0.35)
$\pi\rightarrow\pi^\star$	3.94 (0.34)	$\pi\rightarrow\pi^\star$	3.93 (0.06)	$\pi\rightarrow\pi^\star$	4.00 ($2{\cdot}10^{-3}$)
$\pi\rightarrow\pi^\star$	4.68	$\pi\rightarrow\pi^\star$	4.64	$\pi\rightarrow\pi^\star$	4.64
$\pi\rightarrow\pi^\star$	5.00 (0.43)	$\pi\rightarrow$**wat/Rs**	**4.80**	$\pi\rightarrow\pi^\star$	4.99 (0.34)
$\pi\rightarrow\pi^\star$	5.03	$\pi\rightarrow\pi^\star$	5.00 (0.36)	$\pi\rightarrow\pi^\star$	5.05 (0.06)
$\pi\rightarrow$Rs	5.11	$\pi\rightarrow\pi^\star$	5.02 (0.02)	$\pi\rightarrow$**Rs/wat**	**5.22**
$\pi\rightarrow$Rpy	5.39	$\pi\rightarrow$**Rs/wat**	**5.06**	$\pi\rightarrow\pi^\star$	5.43 ($2{\cdot}10^{-3}$)
$\pi\rightarrow$Rpz	5.42	$\pi\rightarrow$Rpy,pz	5.23	$\pi\rightarrow$Rpy	5.55 (10^{-3})
$\pi\rightarrow\pi^\star$	5.44	$\pi\rightarrow\pi^\star$	5.36	$\pi\rightarrow$Rpz	5.56
$\pi\rightarrow\pi^\star$	5.61	$\pi\rightarrow$Rpx	5.46 ($2{\cdot}10^{-3}$)	$\pi\rightarrow\pi^\star$	5.63 (0.03)
$\pi\rightarrow\pi^\star$	5.61 (1.02)	$\pi\rightarrow$Rd	5.48	$\pi\rightarrow\pi^\star$	5.64 (0.92)
$\pi\rightarrow$Rpx	5.69 (10^{-3})	$\pi\rightarrow\pi^\star$	5.59 ($3{\cdot}10^{-3}$)	$\pi\rightarrow$Rpx	5.85 (10^{-3})
$\pi\rightarrow$Rd	5.81	$\pi\rightarrow$Rd	5.60	$\pi\rightarrow$Rd	5.87
$\pi\rightarrow$Rd	5.82	$\pi\rightarrow$Rd	5.63	$\pi\rightarrow\pi^\star$	5.90
$\pi\rightarrow$Rd	5.83	$\pi\rightarrow\pi^\star$	5.64 (0.98)	π(+nO)$\rightarrow\pi^\star$	5.96
$\pi\rightarrow\pi^\star$	5.88	$\pi\rightarrow$Rd	5.79 ($2{\cdot}10^{-3}$)	$\pi\rightarrow$Rd	5.96
$\pi\rightarrow\pi^\star$	5.99	$\pi\rightarrow$**wat/Rs**	**5.86 (10^{-3})**	$\pi\rightarrow\pi^\star$	5.99
VIP (eV)	7.28		6.97		7.48
Nb(H–C)			0		7
Nb(O–H)			2		0

4 Discussion

We showed in section 3.2 that, in the case of corannulene-water clusters, no $\pi\rightarrow$R/wat transition is observed for the 3-cav geometry formed in the matrix, neither for the 2-cav, and with an extremely minor contribution for the 2-vex, whose presence could not be excluded in the matrix [16]. This can account for the absence of reactivity. As explained in section 3.2, some virtual orbitals of the NTOs appear to have small contributions on the diffuse orbitals of the H atoms closest to corannulene, mostly for the "side" conformations, but their weight appears much smaller than in the case of pyrene. Therefore in the case of corannulene, for the conformers formed in the matrix, the population of PAH^+-H_2O^- CT states is not expected under low energy irradiation ($\lambda > 235$ nm or $\Delta E < 5.28$ eV).

On the opposite, as shown in section 3.3, $\pi\rightarrow$R/wat transitions are observed for all $C_{16}H_{10}(H_2O)_n$ clusters. Contrary to the case of corannulene, the geometries

Table 7 Pyrene + $2H_2O$. TD-DFT CAM-B3LYP excitation energies (eV) and, in parenthesis, oscillator strengths. /wat means that the MO also involves H and, to lesser extent, O diffuse atomic orbitals of the water molecules.. The VIP values (in eV) and the number of bonds shorter than 3Å between the H (resp. O) atoms of the water molecules and the C (resp. H) atoms of pyrene (Nb(H–C) (resp. Nb(O–H)) are also reported. R stands for "Rydberg orbitals". The transitions to states developed on both /wat and Rydberg orbitals are reported in bold characters.

Bare		GEO2_IP$_{Min}$ (side+face)		GEO2_IP$_{Max}$ (face)	
$\pi\rightarrow\pi^\star$	3.92	π (+n$_O$)$\rightarrow\pi^\star$	3.90 (0.34)	π(+n$_O$)$\rightarrow\pi^\star$	3.89 (0.34)
$\pi\rightarrow\pi^\star$	3.94 (0.34)	$\pi\rightarrow\pi^\star$	3.92 ($2{\cdot}10^{-3}$)	$\pi\rightarrow\pi^\star$	3.92 ($5{\cdot}10^{-3}$)
$\pi\rightarrow\pi^\star$	4.68	$\pi\rightarrow\pi^\star$	4.61 ($2{\cdot}10^{-3}$)	$\pi\rightarrow\pi^\star$	4.65 ($2{\cdot}10^{-3}$)
$\pi\rightarrow\pi^\star$	5.00 (0.43)	$\pi\rightarrow\pi^\star$	4.97 (0.41)	$\pi\rightarrow\pi^\star$	4.96 (0.34)
$\pi\rightarrow\pi^\star$	5.03	$\pi\rightarrow\pi^\star$	5.04 (0.02)	$\pi\rightarrow\pi^\star$	5.00 (0.07)
$\pi\rightarrow$Rs	5.11	$\pi\rightarrow$**Rs/wat**	**5.11 ($3{\cdot}10^{-3}$)**	$\pi\rightarrow$**Rs/wat**	**5.30**
$\pi\rightarrow$Rpy	5.39	$\pi\rightarrow$**Rpy/wat**/$\pi^\star$	**5.38 ($2{\cdot}10^{-3}$)**	$\pi\rightarrow\pi^\star$	5.44 ($2{\cdot}10^{-3}$)
$\pi\rightarrow$Rpz	5.42	$\pi\rightarrow$**Rpy/wat**/$\pi^\star$	**5.46 ($5{\cdot}10^{-3}$)**	$\pi\rightarrow\pi^\star$/Rp	5.61 (0.33)
$\pi\rightarrow\pi^\star$	5.44	$\pi\rightarrow$Rpz	5.58 (10^{-3})	$\pi\rightarrow\pi^\star$/Rp	5.62 (0.11)
$\pi\rightarrow\pi^\star$	5.61	$\pi\rightarrow\pi^\star$	5.61 (0.06)	$\pi\rightarrow\pi^\star$/Rp	5.63 (0.51)
$\pi\rightarrow\pi^\star$	5.61 (1.02)	$\pi\rightarrow\pi^\star$	5.65 (0.90)	$\pi\rightarrow$Rpz	5.66 (0.01)
$\pi\rightarrow$Rpx	5.69 (10^{-3})	$\pi\rightarrow$Rpx	5.78 ($3{\cdot}10^{-3}$)	$\pi\rightarrow\pi^\star$	5.88 ($2{\cdot}10^{-3}$)
$\pi\rightarrow$Rd	5.81	$\pi\rightarrow$Rd	5.87	$\pi\rightarrow$Rpx	5.92 (10^{-3})
$\pi\rightarrow$Rd	5.82	$\pi\rightarrow\pi^\star$	5.88 (10^{-3})	$\pi\rightarrow\pi^\star$	5.95 ($8{\cdot}10^{-3}$)
$\pi\rightarrow$Rd	5.83	$\pi\rightarrow$Rd	5.94 (10^{-3})	$\pi\rightarrow$Rd	6.06
$\pi\rightarrow\pi^\star$	5.88	$\pi\rightarrow\pi^\star$	5.96 ($5{\cdot}10^{-3}$)	$\pi\rightarrow$Rd	6.07
$\pi\rightarrow\pi^\star$	5.99	$\pi\rightarrow$Rd	6.02	$\pi\rightarrow$Rd	6.10
VIP (eV)	7.28		7.47		7.60
Nb(H–C)			5		8
Nb(O–H)			2		0

of pyrene in interaction with small water clusters have not been optimised inside the matrix. The case n=1 is a model case, showing that a low energy $\pi\rightarrow$wat/R transition is found for the "side" GEO1_IP$_{Min}$ isomer below 5 eV. However, for our model system, the oscillator strength is zero. Nevertheless, from our study on coronene, a planar compact PAH slightly larger than pyrene, such side isomers are expected to be formed in the matrix [15] and to be photoreactive [12]. So it may be expected that more than one water molecule could interact with pyrene in the matrix and/or that the influence of the environment would lead to an increase of the oscillator strength, in favor of the formation of a PAH^+-H_2O^- CT state. Indeed, for the "side" GEO1_IP$_{Min}$ isomer , the oscillator strength is zero, but for GEO3_IP$_{Min}$, there is one "side" molecule and the presence of two other molecules leads to an increase of the oscillator strength of a transition whose main /wat contribution is located on the "side" water molecule (see NTO 4 on Fig. 7). So the formation of a low energy PAH^+-H_2O^- CT state becomes more favorable for three water molecules, one of them having a clear "side" interaction with pyrene.

Table 8 Pyrene + $3H_2O$. TD-DFT CAM-B3LYP excitation energies (eV) and, in parenthesis, oscillator strengths. /wat means that the MO also involves H and, to lesser extent, O diffuse atomic orbitals of the water molecules. The VIP values (in eV) and the number of bonds shorter than 3Å between the H (resp. O) atoms of the water molecules and the C (resp. H) atoms of pyrene (Nb(H–C) (resp. Nb(O–H)) are also reported. R stands for "Rydberg orbitals". The transitions to states developed on both /wat and Rydberg orbitals are reported in bold characters.

Bare		GEO3_IP$_{Min}$ (side+face)		GEO3_IP$_{Max}$ (face))	
$\pi\rightarrow\pi^\star$	3.92	π (+n$_O$) $\rightarrow\pi^\star$	3.90 (0.34)	π (+n$_O$)$\rightarrow\pi^\star$	3.91 (0.33)
$\pi\rightarrow\pi^\star$	3.94 (0.34)	$\pi\rightarrow\pi^\star$	3.92 ($3{\cdot}10^{-3}$)	$\pi\rightarrow\pi^\star$	3.92 ($6{\cdot}10^{-3}$)
$\pi\rightarrow\pi^\star$	4.68	$\pi\rightarrow\pi^\star$	4.59 (10^{-3})	$\pi\rightarrow\pi^\star$	4.63
$\pi\rightarrow\pi^\star$	5.00 (0.43)	$\pi\rightarrow$**Rs/wat**	**4.93 (0.09)**	$\pi\rightarrow\pi^\star$	4.97 (0.43)
$\pi\rightarrow\pi^\star$	5.03	$\pi\rightarrow\pi^\star$	4.99 (0.34)	$\pi\rightarrow\pi^\star$	5.01 ($3{\cdot}10^{-3}$)
$\pi\rightarrow$Rs	5.11	$\pi\rightarrow\pi^\star$	5.06 (10^{-3})	$\pi\rightarrow$**Rs/wat**	**5.35 (10^{-3}**)
$\pi\rightarrow$Rpy	5.39	$\pi\rightarrow$**R/wat**	**5.33 (10^{-3})**	$\pi\rightarrow\pi^\star$ (+Rp)	5.43 (10^{-3})
$\pi\rightarrow$Rpz	5.42	$\pi\rightarrow$**R/wat**	**5.37 (10^{-3})**	$\pi\rightarrow\pi^\star$/Rp	5.59 (0.01)
$\pi\rightarrow\pi^\star$	5.44	$\pi\rightarrow\pi^\star$/R	5.44 (10^{-3})	$\pi\rightarrow\pi^\star$	5.61 (0.83)
$\pi\rightarrow\pi^\star$	5.61	$\pi\rightarrow\pi^\star$	5.58 (0.01)	$\pi\rightarrow$Rp	5.63 (0.09)
$\pi\rightarrow\pi^\star$	5.61 (1.02)	$\pi\rightarrow\pi^\star$	5.64 (0.92)	$\pi\rightarrow$Rp	5.75 ($2{\cdot}10^{-3}$)
$\pi\rightarrow$Rpx	5.69 (10^{-3})	$\pi\rightarrow$R	5.67 (0.03)	π/wat$\rightarrow\pi^\star$	5.87 (10^{-3})
$\pi\rightarrow$Rd	5.81	$\pi\rightarrow$Rd	5.74 ($5{\cdot}10^{-3}$)	π/wat$\rightarrow\pi^\star$	5.93
$\pi\rightarrow$Rd	5.82	$\pi\rightarrow$R	5.81	$\pi\rightarrow$Rpx/wat	5.98
$\pi\rightarrow$Rd	5.83	$\pi\rightarrow\pi^\star$	5.88 ($2{\cdot}10^{-3}$)	$\pi\rightarrow$Rd	6.13
$\pi\rightarrow\pi^\star$	5.88	$\pi\rightarrow\pi^\star$	5.96 ($3{\cdot}10^{-3}$)	$\pi\rightarrow$Rd	6.17 (10^{-3})
$\pi\rightarrow\pi^\star$	5.99	$\pi\rightarrow$Rd	5.91	$\pi\rightarrow$Rd	6.17
VIP (eV)	7.28		7.34		7.71
Nb(H–C)			5		10
Nb(O–H)			3		0

Although this study does not fully rationalize the photo-reactivity of pyrene with water in a noble gas matrix, it clearly shows that its interaction with a cluster mimicking water ice leads to the presence of low energy transitions with reasonable oscillator strength (below 5 eV) that can be regarded as PAH^+-H_2O^- CT states. Indeed, an increasing number of $\pi\rightarrow$R/wat transitions can be found when the number of water molecules increases for the GEOn_IP $_{Min}$ series. When the number of water molecules becomes large (GEO16_IP $_{Min}$), the transitions mixing $\pi\rightarrow$R/wat and $\pi\rightarrow\pi^\star$ excitations are low in energy and possess a large oscillator strength. Such transitions could be involved in an efficient charge transfer. It is in line with the increase of the reactivity efficiency from matrix experiments, where a few water molecules are involved, to water ice systems where the enhanced efficiency of the PAH reactivity with water in porous amorphous ice was interpreted by the favorable interaction of PAH with water molecules at the surface of cavities [11].

Table 9 Pyrene + nH_2O (n=15,16). TD-DFT CAM-B3LYP excitation energies (eV) and, in parenthesis, oscillator strengths. /wat means that the MO also involves H and, to lesser extent, O diffuse atomic orbitals of the water molecules. The VIP values (in eV) and the number of bonds shorter than 3Å between the H (resp. O) atoms of the water molecules and the C (resp. H) atoms of pyrene (Nb(H–C) (resp. Nb(O–H)) are also reported. R stands for "Rydberg orbitals".

Bare		GEO16_IP$_{Min}$		GEO15_IP$_{Max}$	
$\pi\rightarrow\pi^\star$	3.92	$\pi\rightarrow\pi^\star$	3.82 (0.35)	$\pi\rightarrow\pi^\star$	3.91 (0.30)
$\pi\rightarrow\pi^\star$	3.94 (0.34)	$\pi\rightarrow\pi^\star$	3.89 ($4{\cdot}10^{-3}$)	$\pi\rightarrow\pi^\star$	3.96 (0.04)
$\pi\rightarrow\pi^\star$	4.68	$\pi\rightarrow$**R/wat**	**4.19 (0.0)**	$\pi\rightarrow\pi^\star$	4.60 (0.0)
$\pi\rightarrow\pi^\star$	5.00 (0.43)	$\pi\rightarrow$**Rpx/wat** **($+\pi^\star$)**	**4.48 (0.0)**	$\pi\rightarrow\pi^\star$	4.97 (0.38)
$\pi\rightarrow\pi^\star$	5.03	$\pi\rightarrow\pi^\star$ **(+R/wat)**	**4.52 (0.002)**	$\pi\rightarrow\pi^\star$	5.07 ($3{\cdot}10^{-3}$)
$\pi\rightarrow$Rs	5.11	$\pi\rightarrow\ \pi^\star$**/wat**	**4.55 (0.002)**	$\pi\rightarrow\pi^\star$ + **R/wat**	**5.45 ($5{\cdot}10^{-3}$)**
$\pi\rightarrow$Rpy	5.39	$\pi\rightarrow$**R/wat** + $\pi^\star$	**4.89 (0.18)**	$\pi\rightarrow$**wat/R**	**5.47 (0.0)**
$\pi\rightarrow$Rpz	5.42	$\pi\rightarrow$**R/wat** + $\pi^\star$	4.90 (0.15)	$\pi\rightarrow\pi^\star$	5.61 (0.89)
$\pi\rightarrow\pi^\star$	5.44	$\pi\rightarrow$**R/wat**	5.05 (0.001)	$\pi\rightarrow\pi^\star$	5.62 (0.02)
$\pi\rightarrow\pi^\star$	5.61	$\pi\rightarrow\pi^\star$	5.07 (0.05)	$\pi\rightarrow$**Rp/wat**	**5.75 (10^{-3})**
$\pi\rightarrow\pi^\star$	5.61 (1.02)	$\pi\rightarrow$**R/wat**	5.15 (0.0)	$\pi\rightarrow\pi^\star$	5.90 (0.0)
$\pi\rightarrow$Rpx	5.69 (10^{-3})	$\pi\rightarrow$**R/wat**	**5.22 (0.02)**	$\pi\rightarrow\pi^\star$	5.95 (0.0)
$\pi\rightarrow$Rd	5.81	$\pi\rightarrow$**R/wat**	**5.24 (0.002)**	$\pi\rightarrow$**Rp/wat**	**5.98 (10^{-3})**
$\pi\rightarrow$Rd	5.82	$\pi\rightarrow\pi^\star$**/wat**	**5.30 ($3{\cdot}10^{-3}$)**	$n_O\rightarrow\ \pi^\star$	6.00 (0.0)
$\pi\rightarrow$Rd	5.83	$\pi/$**n**$_O\rightarrow$**/wat**	**5.40 (0.05)**	$\pi\rightarrow$Rd	6.06 (0.0)
$\pi\rightarrow\pi^\star$	5.88	$\pi\rightarrow$R	5.44 ($2{\cdot}10^{-3}$)	$\pi\rightarrow$Rd	6.18 (0.04)
$\pi\rightarrow\pi^\star$	5.99	$\pi\rightarrow\pi^\star$	5.46 (0.05)	$n_O\rightarrow\pi^\star$	6.29 (0.0)
VIP (eV)	7.28		6.54		7.97
Nb(H–C)			7		16
Nb(O–H)			6		1

Another difference between the electronic spectra of corannulene and pyrene in interaction with water clusters is the presence of $n_O\rightarrow\pi^\star$ transitions in the case of corannulene, that do not occur for pyrene, except for GEO15_IP $_{Max}$. Such states, that are also observed for benzene-water clusters [26], can be regarded as CT states from water to PAH, which is once again not in favor of the formation of a PAH^+-H_2O^- CT state.

Finally, this study shows, for a planar PAH:
- in the case of the interaction with one water molecule, the correlation between the low VIP and a "side" interaction with a water molecule close to the PAH (minimum O-H distance of 2.25 Å for GEO1_IP $_{Min}$)
- in the case of pyrene in interaction with an increasing number of water molecules up to reaching a piece of Ih water ice, the correlation between low (resp. high) VIPs, low (resp. high) energy excited states involving $\pi\rightarrow$R/wat

transitions, and the presence of large number of O-H (resp. H-C) interactions.

5 Conclusion

The electronic excited states of corannulene and pyrene in interaction with water molecules and clusters in different arrangements and of various sizes. were investigated at the TD-DFT level of theory up to ∼6 eV. All geometries were obtained at the DFTB level using an adapted hamiltonian. This study demonstrates the dependence of the shape of the PAH, of the arrangements of the water molecules and of the size of the clusters on the electronic spectra.

In the case of pyrene $C_{16}H_{10}$, a planar PAH, two geometries of $C_{16}H_{10}-H_2O$ were locally optimised, a "face" isomer and a "side" isomer. Only in the latter case, where the water molecule interacts in the plane of pyrene via its oxygen atoms (also called σ isomer), a low energy transition involving electron transfer from a π orbital to a diffuse orbital, mainly developed on the water molecule, was found. Such transition can be regarded as a PAH^+-H_2O^- CT state but it has no oscillator strength. Although such conformation is expected to be the one formed in a noble gas matrix matrix, the photo-reactivity of pyrene can only be explained if the oscillator strength is sufficient, which might occur inside the matrix, which has not been explicitly into account in the present work.

The other geometries of $C_{16}H_{10}-(H_2O)_n$ were extracted from pyrene-ice structures, one series leading to a decrease of the VIP (n=2,3,16), the other to an increase of the VIP (n=2,3,15), with respect to pyrene. In the former case, for all geometries, low energy states involving electron transfer from the π orbitals of pyrene to a mix of Rydberg atomic and diffuse molecular orbitals, located mainly on the most external hydrogen atoms of the water clusters, are found. The number of $\pi\rightarrow$R/wat CT states and the corresponding oscillator strengths increase with the size of the water cluster up to n=16, where the water clusters represent a piece of hexagonal ice leading to a decrease of the VIP value with respect to pyrene. Interestingly, these transitions are found more than 2 eV below the VIP of pyrene. Such states could be involved in the photo-reactivity of planar PAHs that were observed to react upon irradiation with low energy photons, and even more efficiently in an icy environment.

Regarding corannulene interacting with water clusters, $\pi\rightarrow$R/wat CT states states were not identified for the 3-cav isomer expected to be formed in the matrix. Such transition was only clearly identified for the 1-side isomer, which is not expected to be formed in the experiment. For the others, the contribution of the water molecules to the diffuse orbital (SAMO or Rydberg or mixed) is minor and is mostly observed for the "side" isomers not expected to be formed in the experiments. This is in line with the absence of observed

photo-reactivity in the case of corannulene.

The results reported in the present paper contribute to the interpretation of experimental results of photo-reactivity of planar vs bowl-shaped PAHs with water in a noble gas matrix or in water ice, and constitute a step forward in understanding photochemical processes for large systems of astrophysical and environmental interest.

6 Acknowledgments

The authors thank Joëlle Mascetti and Jennifer Noble for fruitful scientific discussions. This work has been funded by the French Agence Nationale de la Recherche (ANR) project PARCS ANR-13-BS08-005. For the purpose of open access, the author has applied a CC-BY public copyright licence to any Author Accepted Manuscript (version arising from this submission). This work was also supported by the French research network EMIE (Edifices Moléculaires Isolés et Environnés, GDR 3533), and by the French National Program Physique et Chimie du Milieu Interstellaire (PCMI) of the CNRS/INSU with the INC/INP, co-funded by the CEA and the CNES.

References

1. J. H. Seinfeld and S. N. Pandis, Atmospheric Chemistry and Physics: From Air Pollution to Climate Change. John Wiley & Sons Inc.:Hoboken, NJ, 2016.
2. I. S. Vinklárek, A. Pysanenko, E. Pluhařová, and M. Fárník, "Uptake of Hydrogen Bonding Molecules by Benzene Nanoparticles," J. Phys. Chem. lett., vol. 13, pp. 3781–3788, May 2022. Publisher: American Chemical Society.
3. A. R. Ravishankara, "Heterogeneous and multiphase chemistry in the troposphere," Science, vol. 276, no. 5315, pp. 1058–1065, 1997.
4. C. George, M. Ammann, B. D'Anna, D. J. Donaldson, and S. A. Nizkorodov, "Heterogeneous photochemistry in the atmosphere," Chemical Reviews, vol. 115, no. 10, pp. 4218–4258, 2015.
5. L. J. Allamandola, A. G. G. M. Tielens, and J. R. Barker, "Polycyclic aromatic-hydrocarbons and the unidentified infrared-emission bands - auto exhaust along the milky-way," Astrophys. J., vol. 290, no. 1, pp. L25–L28, 1985.
6. A. Léger and J. L. Puget, "Identification of the 'unidentified' IR emission features of interstellar dust?," Astron. Astrophys., vol. 137, pp. L5–L8, 1984.
7. L. J. Allamandola, A. G. Tielens, and J. R. Barker, "Interstellar polycyclic aromatic hydrocarbons: the infrared emission bands, the excitation/emission mechanism, and the astrophysical implications.," Astrophys J Suppl Ser, vol. 71, pp. 733–775, 1989.
8. A. Tielens, "Interstellar polycyclic aromatic hydrocarbon molecules," Ann. Rev. Astron. Astrophys., vol. 46, no. 1, pp. 289–337, 2008.
9. B. A. McGuire, R. A. Loomis, A. M. Burkhardt, K. L. K. Lee, C. N. Shingledecker, S. B. Charnley, I. R. Cooke, M. A. Cordiner, E. Herbst, S. Kalenskii, M. A. Siebert, E. R. Willis, C. Xue, A. J. Remijan, and M. C. McCarthy, "Detection of two interstellar polycyclic aromatic hydrocarbons via spectral matched filtering.," Science, vol. 371, pp. 1265–1269, 2021.
10. J. Bouwman, A. L. Mattioda, H. Linnartz, and L. J. Allamandola, "Photochemistry of pahs in cosmic water ice i. mid-ir spectroscopy and photoproducts," Astron. Astrophys, vol. 525, p. A93, 2011.

11. Noble, J. A., Michoulier, E., Aupetit, C., and Mascetti, J., "Influence of ice structure on the soft uv photochemistry of pahs embedded in solid water," Astron. Astrophys., vol. 644, p. A22, 2020.
12. Z. Guennoun, C. Aupetit, and J. Mascetti, "Photochemistry of coronene with water at 10 K: first tentative identification by infrared spectroscopy of oxygen containing coronene products," Phys. Chem. Chem. Phys., vol. 13, no. 16, pp. 7340–7347, 2011.
13. Z. Guennoun, C. Aupetit, and J. Mascetti, "Photochemistry of Pyrene with Water at Low Temperature: Study of Atmospherical and Astrochemical Interest," J. Phys. Chem. A, vol. 115, pp. 1844–1852, MAR 17 2011.
14. J. A. Noble, C. Jouvet, C. Aupetit, A. Moudens, and J. Mascetti, "Efficient photochemistry of coronene:water complexes," Astron. Astrophys., vol. 599, p. A124, MAR 2017.
15. A. Simon, J. A. Noble, G. Rouaut, A. Moudens, C. Aupetit, C. Iftner, and J. Mascetti, "Formation of coronene: water complexes: Ftir study in argon matrices and theoretical characterisation," Phys. Chem. Chem. Phys., vol. 19, pp. 8516–8529, MAR 2017.
16. H. Leboucher, J. Mascetti, C. Aupetit, J. A. Noble, and A. Simon, "Water Clusters in Interaction with Corannulene in a Rare Gas Matrix: Structures, Stability and IR Spectra," Photochem, vol. 2, pp. 237–262, Mar. 2022.
17. C. Pérez, A. L. Steber, A. M. Rijs, B. Temelso, G. C. Shields, J. C. Lopez, Z. Kisiel, and M. Schnell, "Corannulene and its complex with water: a tiny cup of water," Phys. Chem. Chem. Phys., vol. 19, pp. 14214–14223, 2017.
18. A. K. Lemmens, S. Gruet, A. L. Steber, J. Antony, S. Grimme, M. Schnell, and A. M. Rijs, "Far-ir and uv spectral signatures of controlled complexation and microhydration of the polycyclic aromatic hydrocarbon acenaphthene," Phys. Chem. Chem. Phys., vol. 21, pp. 3414–3422, 2019.
19. D. Loru, A. L. Steber, P. Pinacho, S. Gruet, B. Temelso, A. M. Rijs, C. Perez, and M. Schnell, "How does the composition of a pah influence its microsolvation? a rotational spectroscopy study of the phenanthrene–water and phenanthridine–water clusters," Phys. Chem. Chem. Phys., vol. 23, pp. 9721–9732, 2021.
20. J. Bouwman, D. M. Paardekooper, H. M. Cuppen, H. Linnartz, and L. J. Allamandola, "Real-time optical spectroscopy of vacuum ultraviolet irradiated pyrene:h2o interstellar ice," Astrophys. J., vol. 700, no. 1, p. 56, 2009.
21. M. Gudipati and L. Allamandola, "Polycyclic aromatic hydrocarbon ionization energy lowering in water ices," Astrophys. J., vol. 615, pp. L177–L180, NOV 10 2004.
22. D. Woon and J. Park, "Photoionization of benzene and small polycyclic aromatic hydrocarbons in ultraviolet-processed astrophysical ices: A computational study," Astrophys. J., vol. 607, pp. 342–345, MAY 20 2004.
23. M. Gudipati and L. Allamandola, "Unusual stability of polycyclic aromatic hydrocarbon radical cations in amorphous water ices up to 120 K: Astronomical implications," Astrophys. J., vol. 638, pp. 286–292, FEB 10 2006.
24. E. Michoulier, N. Ben Amor, M. Rapacioli, J. A. Noble, J. Mascetti, C. Toubin, and A. Simon, "Theoretical determination of adsorption and ionisation energies of polycyclic aromatic hydrocarbons on water ice," Phys. Chem. Chem. Phys., vol. 20, no. 17, pp. 11941–11953, 2018.
25. Y. V. Novakovskaya and N. F. Stepanov, "Nonempirical description of the atmospherically important anionic species. i. water cluster anions," Struct. Chem., vol. 15, pp. 65–70, 2004.
26. N. Ben Amor, E. Michoulier, and A. Simon, "Electronic excited states of benzene in interaction with water clusters: influence of structure and size: Time dependent density functional theory vs multireference wavefunction approaches.," Theo. Chem. Acc., vol. 140, p. 70, June 2021.
27. J. Finley, P.-Å. Malmqvist, B. O. Roos, and L. Serrano-Andrés, "The multi-state CASPT2 method," Chem. Phys. Lett., vol. 288, pp. 299–306, May 1998.
28. C. Iftner, A. Simon, K. Korchagina, M. Rapacioli, and F. Spiegelman, "A density functional tight binding/force field approach to the interaction of molecules with rare gas clusters: Application to $(c6h6)^{+/0}ar_n$ clusters," J. Chem. Phys., vol. 140, no. 3, pp. –, 2014.

29. A. Simon, C. Iftner, J. Mascetti, and F. Spiegelman, "Water clusters in an argon matrix: Infrared spectra from molecular dynamics simulations with a self-consistent charge density functional-based tight binding/force-field potential," J. Phys. Chem A, vol. 119, pp. 2449–2467, 2015.
30. J. A. Noble, C. Aupetit, D. Descamps, S. Petit, A. Simon, J. Mascetti, N. Ben Amor, and V. Blanchet, "Ultrafast electronic relaxations from the S 3 state of pyrene," Phys. Chem. Chem. Phys., vol. 21, no. 26, pp. 14111–14125, 2019.
31. T. H. Dunning and P. J. Hay, "Gaussian basis sets for molecular calculations," in Methods of Electronic Structure Theory (H. F. Schaefer, ed.), pp. 1–27, Springer US, 1977.
32. P. Čàrsky and M. Urban, Ab Initio Calculations: Methods and Applications in Chemistry, vol. 16 of Lecture Notes in Chemistry. Springer Berlin Heidelberg, 1980.
33. R. Krishnan, J. S. Binkley, R. Seeger, and J. A. Pople, "Self-consistent molecular orbital methods. XX. A basis set for correlated wave functions," J. Chem. Phys., vol. 72, pp. 650–654, Jan. 1980.
34. T. Clark, J. Chandrasekhar, G. W. Spitznagel, and P. V. R. Schleyer, "Efficient diffuse function-augmented basis sets for anion calculations. III. The 3-21+G basis set for first-row elements, Li-F," J. Comput. Chem., vol. 4, no. 3, pp. 294–301, 1983.
35. P.-O. Widmark, P.-Å. Malmqvist, and B. O. Roos, "Density matrix averaged atomic natural orbital (ANO) basis sets for correlated molecular wave functions: I. first row atoms," Theor. Chim. Acta, vol. 77, no. 5, pp. 291–306, 1990.
36. P. J. Stephens, F. J. Devlin, C. F. Chabalowski, and M. J. Frisch, "Ab Initio Calculation of Vibrational Absorption and Circular Dichroism Spectra Using Density Functional Force Fields," J. Phys. Chem., vol. 98, pp. 11623–11627, Nov. 1994.
37. S. H. Vosko, L. Wilk, and M. Nusair, "Accurate spin-dependent electron liquid correlation energies for local spin density calculations: a critical analysis," Canadian Journal of Physics, vol. 58, pp. 1200–1211, Aug. 1980.
38. A. D. Becke, "Density-functional thermochemistry. III. The role of exact exchange," J. Chem. Phys., vol. 98, pp. 5648–5652, Apr. 1993.
39. C. Lee, W. Yang, and R. G. Parr, "Development of the Colle-Salvetti correlation-energy formula into a functional of the electron density," Phys. Rev. B, vol. 37, pp. 785–789, Jan. 1988.
40. T. Yanai, D. P. Tew, and N. C. Handy, "A new hybrid exchange–correlation functional using the Coulomb-attenuating method (CAM-B3LYP)," Chem. Phys. Lett., vol. 393, pp. 51–57, July 2004.
41. Y. Zhao and D. G. Truhlar, "The M06 suite of density functionals for main group thermochemistry, thermochemical kinetics, noncovalent interactions, excited states, and transition elements: two new functionals and systematic testing of four M06-class functionals and 12 other functionals," Theo. Chem. Acc., vol. 120, no. 1, pp. 215–241, 2008.
42. J.-D. Chai and M. Head-Gordon, "Systematic optimization of long-range corrected hybrid density functionals," J. Chem. Phys., vol. 128, p. 084106, Feb. 2008.
43. B. O. Roos, P. R. Taylor, and P. E. Siegbahn, "A complete active space SCF method (CASSCF) using a density matrix formulated super-CI approach," Chem. Phys., vol. 48, pp. 157–173, May 1980.
44. J. Olsen, B. O. Roos, P. JÃ¸rgensen, and H. J. A. Jensen, "Determinant based configuration interaction algorithms for complete and restricted configuration interaction spaces," J. Chem. Phys., vol. 89, pp. 2185–2192, Aug. 1988.
45. P.-Å. Malmqvist, A. Rendell, and B. O. Roos, "The restricted active space self-consistent-field method, implemented with a split graph unitary group approach," J. Phys. Chem., vol. 94, pp. 5477–5482, July 1990. Publisher: American Chemical Society.
46. P.-Å. Malmqvist, K. Pierloot, A. R. M. Shahi, C. J. Cramer, and L. Gagliardi, "The restricted active space followed by second-order perturbation theory method: Theory and application to the study of CuO2 and Cu2O2 systems," J. Chem. Phys., vol. 128, no. 20, p. 204109, 2008.
47. V. Sauri, L. Serrano-AndrÃ©s, A. R. M. Shahi, L. Gagliardi, S. Vancoillie, and K. Pierloot, "Multiconfigurational Second-Order Perturbation Theory Restricted Active Space (RASPT2) Method for Electronic Excited States: A Benchmark Study," J. Chem. Theo. Comput., vol. 7, pp. 153–168, Jan. 2011.

48. F. Aquilante, L. De Vico, N. Ferré, G. Ghigo, P.-Å. Malmqvist, P. Neogrády, T. B. Pedersen, M. Pitoňák, M. Reiher, B. O. Roos, L. Serrano-Andrés, M. Urban, V. Veryazov, and R. Lindh, "Molcas 7: The next generation," J. Comput. Chem., vol. 31, no. 1, pp. 224–247, 2010.
49. V. Veryazov, P.-O. Widmark, L. Serrano-Andrés, R. Lindh, and B. O. Roos, "2molcas as a development platform for quantum chemistry software," Int. J. Quantum Chem., vol. 100, no. 4, pp. 626–635, 2004.
50. G. Karlström, R. Lindh, P.-Å. Malmqvist, B. O. Roos, U. Ryde, V. Veryazov, P.-O. Widmark, M. Cossi, B. Schimmelpfennig, P. Neogrady, and L. Seijo, "Molcas: a program package for computational chemistry," Comput. Mat. Science, vol. 28, pp. 222–239, 10 2003.
51. R. L. Martin, "Natural transition orbitals," J. Chem. Phys., vol. 118, pp. 4775–4777, Mar. 2003.
52. M. J. Frisch, G. W. Trucks, H. B. Schlegel, G. E. Scuseria, M. A. Robb, J. R. Cheeseman, G. Scalmani, V. Barone, G. A. Petersson, H. Nakatsuji, X. Li, M. Caricato, A. V. Marenich, J. Bloino, B. G. Janesko, R. Gomperts, B. Mennucci, H. P. Hratchian, J. V. Ortiz, A. F. Izmaylov, J. L. Sonnenberg, D. Williams-Young, F. Ding, F. Lipparini, F. Egidi, J. Goings, B. Peng, A. Petrone, T. Henderson, D. Ranasinghe, V. G. Zakrzewski, J. Gao, N. Rega, G. Zheng, W. Liang, M. Hada, M. Ehara, K. Toyota, R. Fukuda, J. Hasegawa, M. Ishida, T. Nakajima, Y. Honda, O. Kitao, H. Nakai, T. Vreven, K. Throssell, J. A. Montgomery, Jr., J. E. Peralta, F. Ogliaro, M. J. Bearpark, J. J. Heyd, E. N. Brothers, K. N. Kudin, V. N. Staroverov, T. A. Keith, R. Kobayashi, J. Normand, K. Raghavachari, A. P. Rendell, J. C. Burant, S. S. Iyengar, J. Tomasi, M. Cossi, J. M. Millam, M. Klene, C. Adamo, R. Cammi, J. W. Ochterski, R. L. Martin, K. Morokuma, O. Farkas, J. B. Foresman, and D. J. Fox, "GaussianËœ16 Revision B.01," 2016. Gaussian Inc. Wallingford CT.
53. R. S. Becker, I. S. Singh, and E. A. Jackson, "Comprehensive Spectroscopic Investigation of Polynuclear Aromatic Hydrocarbons. I. Absorption Spectra and State Assignments for the Tetracyclic Hydrocarbons and their Alkyl-Substituted Derivatives," J. Chem. Phys., vol. 38, pp. 2144–2171, May 1963.
54. DMS UV Atlas of Organic Compounds. Verlag Chemie, Weinheim, and Butterworths London, 1971.
55. P. Salvi, P. Foggi, and E. Castellucci, "The two-photon excitation spectrum of pyrene," Chem. Phys. Lett., vol. 98, pp. 206–211, June 1983.
56. C. M. Jones and S. A. Asher, "Ultraviolet resonance Raman study of the pyrene S 4 , S 3 , and S 2 excited electronic states," J. Chem. Phys., vol. 89, pp. 2649–2661, Sept. 1988.
57. A. Thöny and M. J. Rossi, "Gas-phase UV spectroscopy of anthracene, xanthone, pyrene, 1-bromopyrene and 1,2,4-trichlorobenzene at elevated temperatures," J. Photochem. Photobiol A, vol. 104, pp. 25–33, Apr. 1997.
58. M. Baba, M. Saitoh, Y. Kowaka, K. Taguma, K. Yoshida, Y. Semba, S. Kasahara, T. Yamanaka, Y. Ohshima, Y.-C. Hsu, and S. H. Lin, "Vibrational and rotational structure and excited-state dynamics of pyrene," J. Chem. Phys., vol. 131, p. 224318, Dec. 2009.
59. Y. Numata, Y. Suzuki, and I. Suzuka, "Anomalous fluorescence from the second excited singlet state upon excitation to the S4 state of pyrene in a supersonic jet," J. Photochem. Photobiol. A, vol. 237, pp. 49–52, June 2012.
60. G. Rouillé, C. Jäger, M. Steglich, F. Huisken, T. Henning, G. Theumer, I. Bauer, and H.-J. Knölker, "IR, Raman, and UV/Vis Spectra of Corannulene for Use in Possible Interstellar Identification," ChemPhysChem, vol. 9, pp. 2085–2091, Oct. 2008.
61. M. Feng, J. Zhao, and H. Petek, "Atomlike, Hollow-Core–Bound Molecular Orbitals of C_{60}," Science, vol. 320, pp. 359–362, Apr. 2008.
62. M. Feng, J. Zhao, T. Huang, X. Zhu, and H. Petek, "The Electronic Properties of Superatom States of Hollow Molecules," Accounts of Chemical Research, vol. 44, pp. 360–368, May 2011.
63. J. O. Johansson, G. G. Henderson, F. Remacle, and E. E. B. Campbell, "Angular-resolved Photoelectron Spectroscopy of Superatom Orbitals of Fullerenes," Phys. Rev. Lett., vol. 108, p. 173401, Apr. 2012.

64. B. Mignolet, J. O. Johansson, E. E. B. Campbell, and F. Remacle, "Probing Rapidly Ionizing Super Atom Molecular Orbitals in C $_{60}$: A Computational and Femtosecond Photoelectron Spectroscopy Study," ChemPhysChem, vol. 14, pp. 3332–3340, Oct. 2013.
65. J. Zhao, M. Feng, J. Yang, and H. Petek, "The Superatom States of Fullerenes and Their Hybridization into the Nearly Free Electron Bands of Fullerites," ACS Nano, vol. 3, pp. 853–864, Apr. 2009.
66. L. Zoppi, L. Martin-Samos, and K. K. Baldridge, "Buckybowl superatom states: a unique route for electron transport?," Phys. Chem. Chem. Phys., vol. 17, no. 8, pp. 6114–6121, 2015.
67. L. Turi and P. J. Rossky, "Theoretical Studies of Spectroscopy and Dynamics of Hydrated Electrons," Chem Rev., vol. 112, pp. 5641–5674, Nov. 2012.